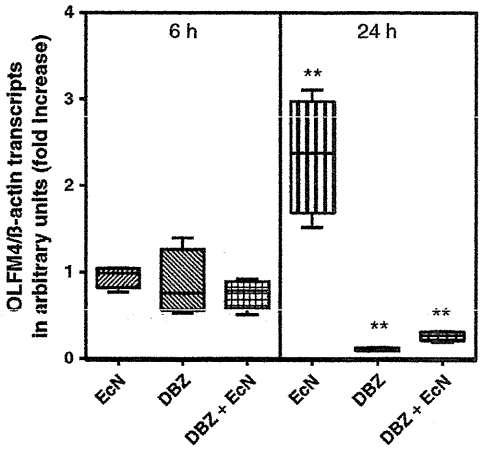

Figure 6 OLFM4 expression in LS174T cells incubated with *E. coli Nissle (EcN)* in the presence and absence of the γ-secretase inhibitor dibenzazepine (DBZ). 24 h of incubation with *EcN* led to a significant increase of OLFM4 transcripts. Treatment with DBZ led to a significant downregulation of OLFM4 transcripts after 24 h. DBZ blocked the stimulation by *EcN*. Values are compared to controls at the given time-point set to 1 (*: $p<0.05$, **: $p<0.01$). This experiment was performed for 4 times in triplicates.

The current study shows that OLFM4 transcripts and also protein are significantly induced in colonic IBD during inflammation. Moreover, OLFM4 expression correlates significantly with that of the proinflammatory cytokine IL-8, but not with the goblet cell differentiation factor Hath1. This implies that OLFM4 expression is triggered by inflammation and not by differentiation, in contrast to mucins.[17] The relative induction of OLFM4 is clearly higher in active UC compared to active CD. In principle, this observation is consistent with the observation of Shinozaki and his group, who found OLFM4 mRNA to be elevated in active vs. inactive UC.[31]

In healthy controls, we found OLFM4 staining to be located primarily in the lower third of the colonic crypt, suggesting that in healthy gut this glycoprotein is not a relevant protective factor in the surface epithelium and mucus. However, during active inflammation OLFM4 immunostaining expanded up to the epithelial surface in IBD samples. Shinozaki et al. detected OLFM4 mRNA signals confined to the crypt epithelial cells by in situ hybridization[31] whereas Clevers and his group[30] found colonic OLFM4 mRNA in humans even restricted to crypt base columnar cells again by in-situ hybridization. It seems possible that in controls the protein expression is retained also in stem cell derived daughter cells colonizing the lower third of the crypt, whereas during inflammation the epithelial cells expressing the protein migrate rapidly up to the surface[39] where it is secreted. This was evident from the presence of OLFM4 protein in the mucus of Carnoy-fixed IBD biopsies, as well as in rectal IBD mucus obtained by endoscopic brushings. Notably, Dot Blot of these mucus extracts was almost free of ß-actin implying that the mucus was not significantly contaminated by cell detritus. The high amino acid sequence similarity between OLFM4 and olfactomedin,[23] the first member of the olfactomedin domain-containing family found to be expressed in the extracellular mucus matrix of olfactory neuroepithelium in bullfrogs,[40–42] also underlines the fate of OLFM4 as a secretory protein.

Moreover, we measured the expression of OLFM4 in relation to the two crucial mucins Muc1 and Muc2. In contrast to unchanged Muc2, Muc1 was induced in both diseases, although somewhat less significant in UC. This is consistent with prior observations showing a compromised mucin synthesis in UC.[17–20] Interestingly, this induction pattern contrasts with OLFM4 expression, which showed a higher induction in UC. It is therefore possible that OLFM4 acts as a mucin substitute complementing the mucus layer during inflammation and bacterial attack.

Since OLFM4 is negatively and HBD1-3 positively charged, binding is probably electrostatic. Both defensins[10] and OLFM4 are located in the mucus, therefore it is plausible that they interact and bind to each other also in vivo in order to concentrate the antimicrobial activity in the mucus. Notably, OLFM4 led only to a minor reduction of the antimicrobial activity of HBD1, HBD2 and HBD3. Thus, OLFM4 appears to function as a glycoprotein binding but not profoundly inactivating defensins. However, it should be noted that recombinant OLFM4 differs from native OLFM4 with respect to its glycosylation.

In addition, we observed OLFM4 transcripts to be induced in LS174T cells after incubation with heat killed *E. coli K12*, *E. coli Nissle* and *B. vulgatus*. Although this is the first description in colonic cells, the principle that specific bacteria may enhance OLFM4 expression was previously demonstrated in the mouse primary gastric epithelial cell line GSM06 incubated with *H. pylori*.[27] Even more pronounced was the induction by IL-22, a susceptibility gene in UC,[43] also compared to the other cytokines tested. The induction of OLFM4 as a mucus glycoprotein is consistent with the recent observation of an IL-22 mediated increase in goblet cell counts and mucin synthesis in experimental animals.[44] This cytokine also increases the innate immunity of several tissues by the induction of antimicrobial peptides such as HBD2 and HBD3.[45] Accordingly, IL-22 was demonstrated to protect mice from colitis,[46] probably by enhancing the mucus/defensin barrier.

Gene expression profiling experiments found OLFM4 to be a target gene of the Notch pathway and thus cell differentiation, proliferation, and immune response to inflammation.[47] We confirmed this observation by cell culture experiments showing that treatment of LS174T cells with the γ-secretase inhibitor DBZ led to a significant downregulation of OLFM4 transcripts. Moreover, the *E. coli Nissle* mediated induction was also blocked by DBZ, pointing out that the bacterial triggered OLFM4 induction depends on the Notch pathway.

In summary, OLFM4 possesses several "mucin-like" properties (negatively charged polymerizing glycoprotein, secreted into mucus, binding to defensins) and is extensively upregulated in inflamed IBD mucosa where it expands up to the surface epithelium and is secreted into the mucus. The induction may be mediated by bacteria via the Notch pathway and through IL-22. OLFM4 is suggested to have a functional protective role in IBD by binding defensins in the mucus.

Conflict of interest

All Authors have no conflict of interest.

Please cite this article as: Gersemann M, et al. Olfactomedin-4 is a glycoprotein secreted into mucus in active IBD, *Journal of Crohn's and Colitis* (2011), doi:10.1016/j.crohns.2011.09.013

Acknowledgment

The scientific input by Robert Küchler and the technical help by Nadine Krüger, Jutta Bader, Marion Schiffmann, Dagmar Weller, Michelle Katajew, and Kathleen Siegel are gratefully acknowledged.

This research work is supported by the Robert Bosch Foundation, Stuttgart, Germany and the Emmy Noether program (J.W.) of the Deutsche Forschungsgemeinschaft (DFG).

References

1. Sartor RB. Microbial influences in inflammatory bowel diseases. *Gastroenterology* 2008;**134**:577–94.
2. Schreiber S, Rosenstiel P, Albrecht M, Hampe J, Krawczak M. Genetics of Crohn disease, an archetypal inflammatory barrier disease. *Nat Rev Genet* 2005;**6**:376–88.
3. Gersemann M, Wehkamp J, Fellermann K, Stange EF. Crohn's disease–defect in innate defence. *World J Gastroenterol* 2008;**14**:5499–503.
4. Gersemann M, Stange EF, Wehkamp J. From intestinal stem cells to inflammatory bowel diseases. *World J Gastroenterol* 2011;**17**:3198–203.
5. Swidsinski A, Weber J, Loening-Baucke V, Hale LP, Lochs H. Spatial organization and composition of the mucosal flora in patients with inflammatory bowel disease. *J Clin Microbiol* 2005;**43**:3380–9.
6. Johansson ME, Larsson JM, Hansson GC. The two mucus layers of colon are organized by the MUC2 mucin, whereas the outer layer is a legislator of host–microbial interactions. *Proc Natl Acad Sci U S A* 2011;**108**(Suppl 1):4659–65.
7. Darfeuille-Michaud A, Neut C, Barnich N, Lederman E, Di Martino P, Desreumaux P, et al. Presence of adherent *Escherichia coli* strains in ileal mucosa of patients with Crohn's disease. *Gastroenterology* 1998;**115**:1405–13.
8. Moussata D, Goetz M, Gloeckner A, Kerner M, Campbell B, Hoffman A, et al. Confocal laser endomicroscopy is a new imaging modality for recognition of intramucosal bacteria in inflammatory bowel disease in vivo. *Gut* 2011;**60**:26–33.
9. Shirazi T, Longman RJ, Corfield AP, Probert CS. Mucins and inflammatory bowel disease. *Postgrad Med J* 2000;**76**:473–8.
10. Meyer-Hoffert U, Hornef MW, Henriques-Normark B, Axelsson LG, Midtvedt T, Pütsep K, et al. Secreted enteric antimicrobial activity localises to the mucus surface layer. *Gut* 2008;**57**:764–71.
11. Wehkamp J, Schmid M, Fellermann K, Stange EF. Defensin deficiency, intestinal microbes, and the clinical phenotypes of Crohn's disease. *J Leukoc Biol* 2005;**77**:460–5.
12. Wehkamp J, Schmid M, Stange EF. Defensins and other antimicrobial peptides in inflammatory bowel disease. *Curr Opin Gastroenterol* 2007;**23**:370–8.
13. Wehkamp J, Harder J, Weichenthal M, Mueller O, Herrlinger KR, Fellermann K, et al. Inducible and constitutive beta-defensins are differentially expressed in Crohn's disease and ulcerative colitis. *Inflamm Bowel Dis* 2003;**9**:215–23.
14. Peyrin-Biroulet L, Beisner J, Wang G, Nuding S, Oommen ST, Kelly D, et al. Peroxisome proliferator-activated receptor gamma activation is required for maintenance of innate antimicrobial immunity in the colon. *Proc Natl Acad Sci U S A* 2010;**107**:8772–7.
15. McCormick DA, Horton LW, Mee AS. Mucin depletion in inflammatory bowel disease. *J Clin Pathol* 1990;**43**:143–6.
16. Pullan RD, Thomas GA, Rhodes M, Newcombe RG, Williams GT, Allen A, et al. Thickness of adherent mucus gel on colonic mucosa in humans and its relevance to colitis. *Gut* 1994;**35**:353–9.
17. Gersemann M, Becker S, Kubler I, Koslowski M, Wang G, Herrlinger KR, et al. Differences in goblet cell differentiation between Crohn's disease and ulcerative colitis. *Differentiation* 2009;**77**:84–94.
18. Hanski C, Born M, Foss HD, Marowski B, Mansmann U, Arastéh K, et al. Defective post-transcriptional processing of MUC2 mucin in ulcerative colitis and in Crohn's disease increases detectability of the MUC2 protein core. *J Pathol* 1999;**188**:304–11.
19. Moehle C, Ackermann N, Langmann T, Aslanidis C, Kel A, Kel-Margoulis O, et al. Aberrant intestinal expression and allelic variants of mucin genes associated with inflammatory bowel disease. *J Mol Med* 2006;**84**:1055–66.
20. Tytgat KM, van der Wal JW, Einerhand AW, Büller HA, Dekker J. Quantitative analysis of MUC2 synthesis in ulcerative colitis. *Biochem Biophys Res Commun* 1996;**224**:397–405.
21. Van Klinken BJ, van der Wal JW, Einerhand AW, Büller HA, Dekker J. Sulphation and secretion of the predominant secretory human colonic mucin MUC2 in ulcerative colitis. *Gut* 1999;**44**:387–93.
22. Liu W, Zhu J, Cao L, Rodgers GP. Expression of hGC-1 is correlated with differentiation of gastric carcinoma. *Histopathology* 2007;**51**:157–65.
23. Zhang J, Liu WL, Tang DC, Chen L, Wang M, Pack SD, et al. Identification and characterization of a novel member of olfactomedin-related protein family, hGC-1, expressed during myeloid lineage development. *Gene* 2002;**283**:83–93.
24. Zhang X, Huang Q, Yang Z, Li Y, Li CY. GW112, a novel antiapoptotic protein that promotes tumor growth. *Cancer Res* 2004;**64**:2474–81.
25. Grover PK, Hardingham JE, Cummins AG. Stem cell marker olfactomedin 4: critical appraisal of its characteristics and role in tumorigenesis. *Cancer Metastasis Rev* 2010;**29**:761–75.
26. Liu W, Chen L, Zhu J, Rodgers GP. The glycoprotein hGC-1 binds to cadherin and lectins. *Exp Cell Res* 2006;**312**:1785–97.
27. Liu W, Yan M, Liu Y, Wang R, Li C, Deng C, et al. Olfactomedin 4 down-regulates innate immunity against *Helicobacter pylori* infection. *Proc Natl Acad Sci U S A* 2010;**107**:11056–61.
28. Mannick EE, Schurr JR, Zapata A, Lentz JJ, Gastanaduy M, Cote RL, et al. Gene expression in gastric biopsies from patients infected with *Helicobacter pylori*. *Scand J Gastroenterol* 2004;**39**:1192–200.
29. Barker N, van Es JH, Kuipers J, Kujala P, van den Born M, Cozijnsen M, et al. Identification of stem cells in small intestine and colon by marker gene Lgr5. *Nature* 2007;**449**:1003–7.
30. van der Flier LG, Haegebarth A, Stange DE, van de Wetering M, Clevers H. OLFM4 is a robust marker for stem cells in human intestine and marks a subset of colorectal cancer cells. *Gastroenterology* 2009;**137**:15–7.
31. Shinozaki S, Nakamura T, Iimura M, Kato Y, Iizuka B, Kobayashi M, et al. Upregulation of Reg 1alpha and GW112 in the epithelium of inflamed colonic mucosa. *Gut* 2001;**48**:623–9.
32. Stange EF, Travis SP, Vermeire S, Reinisch W, Geboes K, Barakauskiene A, et al. European evidence-based consensus on the diagnosis and management of ulcerative colitis: definitions and diagnosis. *J Crohns Colitis* 2008;**2**:1–23.
33. Van Assche G, Dignass A, Panes J, Beaugerie L, Karagiannis J, Allez M, et al. The second European evidence-based consensus on the diagnosis and management of Crohn's disease: definitions and diagnosis. *J Crohns Colitis* 2010;**4**:7–27.
34. Stoscheck CM. Quantitation of protein. *Methods Enzymol* 1990;**182**:50–68.
35. Oue N, Sentani K, Noguchi T, Ohara S, Sakamoto N, Hayashi T, et al. Serum olfactomedin 4 (GW112, hGC-1) in combination with Reg IV is a highly sensitive biomarker for gastric cancer patients. *Int J Cancer* 2009;**125**:2383–92.
36. Schmid M, Fellermann K, Fritz P, Wiedow O, Stange EF, Wehkamp J. Attenuated induction of epithelial and leukocyte serine antiproteases elafin and secretory leukocyte protease inhibitor in Crohn's disease. *J Leukoc Biol* 2007;**81**:907–15.
37. Nuding S, Fellermann K, Wehkamp J, Mueller HA, Stange EF. A flow cytometric assay to monitor antimicrobial activity of

Please cite this article as: Gersemann M, et al. Olfactomedin-4 is a glycoprotein secreted into mucus in active IBD. *Journal of Crohn's and Colitis* (2011), doi:10.1016/j.crohns.2011.09.013

defensins and cationic tissue extracts. *J Microbiol Methods* 2006;**65**:335–45.
38. Schlee M, Harder J, Koten B, Stange EF, Wehkamp J, Fellermann K. Probiotic lactobacilli and VSL#3 induce enterocyte beta-defensin 2. *Clin Exp Immunol* 2008;**151**:528–35.
39. Serafini EP, Kirk AP, Chambers TJ. Rate and pattern of epithelial cell proliferation in ulcerative colitis. *Gut* 1981;**22**:648–52.
40. Bal RS, Anholt RR. Formation of the extracellular mucous matrix of olfactory neuroepithelium: identification of partially glycosylated and nonglycosylated precursors of olfactomedin. *Biochemistry* 1993;**32**:1047–53.
41. Snyder DA, Rivers AM, Yokoe H, Menco BP, Anholt RR. Olfactomedin: purification, characterization, and localization of a novel olfactory glycoprotein. *Biochemistry* 1991;**30**:9143–53.
42. Yokoe H, Anholt RR. Molecular cloning of olfactomedin, an extracellular matrix protein specific to olfactory neuroepithelium. *Proc Natl Acad Sci U S A* 1993;**90**:4655–9.
43. Silverberg MS, Cho JH, Rioux JD, McGovern DP, Wu J, Annese V, et al. Ulcerative colitis-risk loci on chromosomes 1p36 and 12q15 found by genome-wide association study. *Nat Genet* 2009;**41**:216–20.
44. Sugimoto K, Ogawa A, Mizoguchi E, Shimomura Y, Andoh A, Bhan AK, et al. IL-22 ameliorates intestinal inflammation in a mouse model of ulcerative colitis. *J Clin Invest* 2008;**118**:534–44.
45. Wolk K, Kunz S, Witte E, Friedrich M, Asadullah K, Sabat R. IL-22 increases the innate immunity of tissues. *Immunity* 2004;**21**:241–54.
46. Zenewicz LA, Yancopoulos GD, Valenzuela DM, Murphy AJ, Stevens S, Flavell RA. Innate and adaptive interleukin-22 protects mice from inflammatory bowel disease. *Immunity* 2008;**29**:947–57.
47. Rodilla V, Villanueva A, Obrador-Hevia A, Robert-Moreno A, Fernández-Majada V, Grilli A, et al. Jagged1 is the pathological link between Wnt and Notch pathways in colorectal cancer. *Proc Natl Acad Sci U S A* 2009;**106**:6315–20.

Please cite this article as: Gersemann M, et al. Olfactomedin-4 is a glycoprotein secreted into mucus in active IBD. *Journal of Crohn's and Colitis* (2011), doi:10.1016/j.crohns.2011.09.013

Carcinogenesis Advance Access published April 2, 2012
Carcinogenesis vol.0 no.0 pp.1–8, 2012
doi:10.1093/carcin/bgs121
Advance Access publication March 12, 2012

Upregulation of HOXA10 in gastric cancer with the intestinal mucin phenotype: reduction during tumor progression and favorable prognosis

Kazuhiro Sentani, Naohide Oue, Yutaka Naito, Naoya Sakamoto, Katsuhiro Anami, Htoo Zarni Oo, Naohiro Uraoka, Kazuhiko Aoyagi[1], Hiroki Sasaki[1] and Wataru Yasui*

Department of Molecular Pathology, Hiroshima University Graduate School of Biomedical Sciences, Hiroshima, Japan and [1]Division of Genetics, National Cancer Center Research Institute, Tokyo, Japan

*To whom correspondence should be addressed. Tel: +81 82 257 5145; Fax: +81 82 257 5149;
Email: wyasui@hiroshima-u.ac.jp

Gastric cancer (GC) is one of the most common malignancies worldwide. Better knowledge of the changes in gene expression that occur during gastric carcinogenesis may lead to improvements in diagnosis, treatment and prevention. In this study, we screened for genes upregulated in GC by comparing gene expression profiles from microarray and serial analysis of gene expression and identified the *HOXA10* gene. The aim of the present study was to investigate the significance of HOXA10 in GC. Immunohistochemical analysis demonstrated that 221 (30%) of 749 GC cases were positive for HOXA10, whereas HOXA10 was scarcely expressed in non-neoplastic gastric mucosa except in the case of intestinal metaplasia. Next, we analyzed the relationship between HOXA10 expression and clinicopathological characteristics. HOXA10 expression showed a significant inverse correlation with the depth of invasion and was observed more frequently in the differentiated type of GC than in the undifferentiated type of GC. HOXA10 expression was associated with GC with the intestinal mucin phenotype and correlated with CDX2 expression. Furthermore, the prognosis of patients with positive HOXA10 expression was significantly better than in the negative expression cases. 3-(4,5-dimethylthiazole-2-yl)-2,5-diphenyl tetrazolium bromide and wound healing assay revealed that knockdown of HOXA10 in GC cells by short interfering RNA transfection significantly increased viability and motility relative to the negative control, indicating that HOXA10 expression inhibits cell growth and motility. These results suggest that expression of HOXA10 may be a key regulator for GC with the intestinal mucin phenotype.

Introduction

Gastric cancer (GC) is one of the most common human cancers. Cancer develops as a result of multiple genetic and epigenetic alterations (1). Better knowledge of the changes in gene expression that occur during gastric carcinogenesis may lead to improvements in diagnosis, treatment and prevention. Identification of novel biomarkers for cancer diagnosis and novel targets for treatment are major goals in this field (2). We previously performed several large-scale gene expression studies using array-based hybridization (3), serial analysis of gene expression (SAGE) (4,5) and the *Escherichia coli* ampicillin secretion trap (CAST) method (6) and identified several genes including *regenerating islet-derived family, member 4* (*REG4*, which encodes REG IV) (7,8), *palate, lung and nasal epithelium carcinoma-associated protein* (*PLUNC*) (9), *GJB6* (encoding connexin 30) (10) and *DSC2* (encoding desmocollin 2) (11). These results indicated that these methods are useful for identification of novel genes associated with GC; however, such alterations cannot completely explain the pathogenesis of GC. In our previous study, the 20 genes showing the greatest increase in expression on the microarray were quite different from those obtained by SAGE (9). Therefore, we performed gene expression profiling using Affymetrix GeneChip arrays of GC samples previously analyzed by SAGE and identified several candidate GC-associated genes. Among these candidate genes, the *homeobox A10* (*HOXA10*) gene is upregulated in all samples. To date, little is known about the role of HOXA10 in human GC.

The *HOX* genes are important regulators of embryonic morphogenesis and differentiation and control normal development patterning along the anteroposterior axis. They contain a common DNA motif of a sequence of 183 nucleotides, encoding a region of 61 amino acids called the homeodomain, their sequences being the basis for classification into different subsets (12). The homeodomain is responsible for recognizing and binding to sequence-specific DNA motifs and cis regulates the transcription of genes relevant to the formation of specific segmental architecture. In humans, 38 HOXs have been identified that are spread among four different clusters located on four separate chromosomes: 7 (HOXA), 17 (HOXB), 12 (HOXC) and 2 (HOXD) (13). A putative role of HOXs in malignant processes has been well documented in leukemia. They participate in myeloid cell differentiation and proliferation (14,15). HOXA10 and HOXA9 are associated with acute myeloid leukemia and mixed lineage leukemia fusion genes (16). HOXA10 controls uterine organogenesis during embryonic development and endometrial differentiation in adults (17). Deregulation of HOXA10 correlates with progression of endometrial carcinoma (18). CDX2 has been reported to be an upstream regulator for HOXA10 in myeloid cells and participates in leukemogenesis (19). However, the exact pathogenic mechanisms associated with HOXA10 in stomach carcinogenesis remain obscure.

The present study represents the first detailed analysis of HOXA10 expression in GC. To clarify the pattern of expression and localization of HOXA10 in GC, we performed immunohistochemical analysis of surgically resected GC samples and analyzed the association between HOXA10 and various markers including the gastric/intestinal phenotypes (MUC5AC, MUC6, MUC2 and CD10), CDX2, β-catenin, EGFR and p53. Furthermore, we also studied the relationship between HOXA10 expression and patient prognosis and the effect of HOXA10 on cell growth, motility and invasion.

Abbreviations: cDNA, complementary DNA; GC, gastric cancer; RT–PCR, reverse transcription–PCR; SAGE, serial analysis of gene expression; siRNA, short interfering RNA.

Materials and methods

Tissue samples

For microarray analysis, two primary GC samples (W226T: 59-year-old man, T1N0M0, stage I, well-differentiated adenocarcinoma; W246T: 44-year-old man, T2N2M0, stage III, well-differentiated adenocarcinoma) and corresponding non-neoplastic mucosa were used. These GC samples were analyzed previously by SAGE for comprehensive gene expression profiling (5). For quantitative reverse transcription–PCR (RT–PCR) analysis, 38 GC samples and corresponding non-neoplastic mucosa samples were used. The samples were obtained during surgery at the Hiroshima University Hospital. We confirmed microscopically that the tumor specimens were predominantly (>50%) cancer tissue. Samples were frozen immediately in liquid nitrogen and stored at −80°C until use. Samples of normal brain, spinal cord, heart, skeletal muscle, lung, stomach, small intestine, colon, liver, pancreas, kidney, uterus, bone marrow, spleen, peripheral leukocytes and trachea were purchased from Clontech (Palo Alto, CA). For immunohistochemical analysis, we used archival formalin-fixed paraffin-embedded tissues from 749 patients (480 men and 269 women; age range, 29–88 years; mean, 70 years) who had undergone surgical excision for GC at the Hiroshima University Hospital or affiliated hospitals. The 749 GC cases were histologically classified as 429 differentiated type (papillary adenocarcinoma or tubular adenocarcinoma) and 320 undifferentiated type (poorly differentiated adenocarcinoma, signet ring cell carcinoma or mucinous adenocarcinoma), according to the Japanese Classification of Gastric Carcinomas (20). Tumor staging was carried out according to the

International Union Against Cancer TNM classification of malignant tumors. Because written informed consent was not obtained, identifying information for all samples was removed before analysis for strict privacy protection. This procedure was in accordance with the Ethical Guidelines for Human Genome/Gene Research enacted by the Japanese Government.

Microarray analysis

Gene expression profiles of tissue samples were analyzed by genome-wide microarrays as described previously (21). Affymetrix GeneChip Human Genome U133Plus 2.0 arrays (Affymetrix, Santa Clara, CA) were used. Each transcript on this array is represented by a set of 11 probe pairs, called the probe set. The array contains >54 000 probe sets, representing 47 400 transcripts, including 38 500 genes. Five micrograms of total RNA were used to prepare antisense biotinylated RNA with One-cycle Target Labeling and Control Reagent (Affymetrix) according to the manufacturer's instructions. In brief, first-stranded complementary DNA (cDNA) was synthesized with a T7-RNA polymerase promoter-attached oligo(dT) primer followed by second-stranded cDNA synthesis. This cDNA was purified and served as a template in the subsequent *in vitro* T7-transcription. The *in vitro* T7-transcription reaction was carried out in the presence of T7 RNA polymerase and biotinylated UTP for complementary RNA production. The biotinylated complementary RNAs were then cleaned up and fragmented. The fragmented biotinylated complementary RNA was hybridized to the array (45°C for 16 h). The procedures for staining, washing and scanning of arrays were carried out according to the instructions in the Affymetrix technical manual. The expression value (average difference) of each probe was calculated with GeneChip Operating Software Version 1.1 (Affymetrix). The mean of average difference values in each experiment was 1000 to reliably compare variable multiple arrays.

Quantitative RT–PCR analysis

Total RNA was extracted with an RNeasy Mini Kit (Qiagen, Valencia, CA), and 1 μg of total RNA was converted to cDNA with a First Strand cDNA Synthesis Kit (Amersham Biosciences, Piscataway, NJ). Quantitation of *HOXA10* messenger RNA levels in human tissue samples was done by real-time fluorescence detection as described previously (22). PCR was performed with an SYBR Green PCR Core Reagents Kit (Applied Biosystems, Foster City, CA). The *HOXA10* primer sequences were 5′-AGATATTGTCCTAAGTGTCAAGTCCTGA-3′ and 5′-GCCATTTCGAGCAGTGGG-3′. Real-time detection of the emission intensity of SYBR Green bound to double-stranded DNA was performed with an ABI PRISM 7700 Sequence Detection System (Applied Biosystems) as described previously (23). *ACTB*-specific PCR products were amplified from the same RNA samples and served as internal controls. We calculated the ratio of *HOXA10* messenger RNA levels between GC tissue (T) and corresponding non-neoplastic mucosa (N). T/N ratios of >2.0 were considered to indicate upregulation.

Antibodies

Goat polyclonal anti-HOXA10 antibody was purchased from Santa Cruz Biotechnology (Santa Cruz, CA). We used four antibodies for analysis of the GC mucin phenotypes: mouse monoclonal anti-MUC5AC (Novocastra, Newcastle, UK) as a marker of gastric foveolar epithelial cells, mouse monoclonal anti-MUC6 (Novocastra) as a marker of pyloric gland cells, mouse monoclonal anti-MUC2 (Novocastra) as a marker of goblet cells in the small intestine and colorectum and mouse monoclonal anti-CD10 (Novocastra) as a marker of microvilli of absorptive cells in the small intestine and colorectum. In addition, we used mouse monoclonal anti-CDX2 (BioGenex, San Ramon, CA) as a marker of differentiation of intestinal epithelial cells, mouse monoclonal anti-β-catenin (BD Biosciences, San Jose, CA), mouse monoclonal anti-EGFR (Novocastra) and mouse monoclonal anti-p53 (Novocastra).

Western blot analysis

For western blot analysis, tissue samples or cells were lysed as described previously (24). The lysates (40 μg) were solubilized in Laemmli sample buffer by boiling and then subjected to 12% sodium dodecyl sulfate-polyacrylamide gel electrophoresis followed by electrotransfer onto a nitrocellulose filter. Peroxidase-conjugated anti-goat IgG was used in the secondary reaction. Immunocomplexes were visualized with an ECL Western Blot Detection System (Amersham Biosciences). β-actin antibody (Sigma Chemical) was also used as a loading control.

Immunohistochemistry

A Dako LSAB Kit (Dako, Carpinteria, CA) was used for immunohistochemical analysis. In brief, sections were pretreated by microwave treatment in citrate buffer for 15 min to retrieve antigenicity. After peroxidase activity was blocked with 3% H_2O_2 methanol for 10 min, sections were incubated with normal goat serum (Dako) for 20 min to block non-specific antibody binding sites. Sections were incubated with the following primary antibodies: anti-HOXA10 (diluted 1:50), anti-MUC5AC (1:50), anti-MUC6 (1:50), anti-MUC2 (1:50), anti-CD10 (1:50), anti-CDX2 (1:20), anti-β-catenin (1:50), anti-EGFR (1:50) and anti-p53 (1:50). Sections were incubated with primary antibody for 1 h at 25°C, followed by incubations with biotinylated anti-rabbit/mouse IgG and peroxidase-labeled streptavidin for 10 min each. Staining was completed with a 10 min incubation with the substrate-chromogen solution. The sections were counterstained with 0.1% hematoxylin.

Each molecule was classified according to the percentage of stained cancer cells. Expression was considered to be 'negative' if <10% of cancer cells were stained. When at least 10% of cancer cells were stained, the result of immunostaining was considered 'positive'.

Phenotypic analysis of GC

GC cases were classified into four phenotypes: gastric phenotype, intestinal phenotype, gastric and intestinal mixed phenotype and unclassified phenotype. The criteria (25) for classification of gastric phenotype and intestinal phenotype were as follows. GCs in which >10% of the cells displayed the gastric or intestinal epithelial cell phenotype were gastric phenotype or intestinal phenotype cancers, respectively. Those sections that showed both gastric and intestinal phenotypes were classified as gastric and intestinal mixed phenotype, and those that lacked both the gastric and the intestinal phenotypes were classified as the unclassified phenotype.

GC cell lines

Nine cell lines derived from human GC were used. The TMK-1 cell line was established in our laboratory from a poorly differentiated adenocarcinoma (26). Five GC cell lines of the MKN series (MKN-1, adenosquamous cell carcinoma; MKN-7; MKN-28; MKN-74, well-differentiated adenocarcinoma and MKN-45, poorly differentiated adenocarcinoma) were kindly provided by Dr Toshimitsu Suzuki (Fukushima Medical University School of Medicine) (27,28). KATO-III, HSC-39 and HSC-57 cell lines were kindly provided by Dr Morimasa Sekiguchi (University of Tokyo) (29) and Dr Kazuyoshi Yanagihara (Yasuda Women's University) (30), respectively. All cell lines were maintained in RPMI 1640 (Nissui Pharmaceutical Co, Ltd, Tokyo, Japan) containing 10% fetal bovine serum (BioWhittaker, Walkersville, MD) in a humidified atmosphere of 5% CO_2 and 95% air at 37°C.

RNA interference and overexpression of HOXA10 in cell growth, wound healing assay and in vitro *invasion assay*

To knockdown the endogenous *HOXA10*, RNA interference was performed. Short interfering RNA (siRNA) oligonucleotides for *HOXA10* and a negative control were purchased from Invitrogen (Carlsbad, CA). Three independent oligonucleotides were used for *HOXA10* siRNA as follows: a *HOXA10* siRNA1 sequence, 5′-GAGUUUCUGUUCAAUAUGUACCUUA-3′; a *HOXA10* siRNA2 sequence, 5′-CCGGGAGCUCACAGCCAACUUUAAU-3′ and a *HOXA10* siRNA3 sequence, 5′-CGGCAAAGAGUGGUCGGAAGAAGCG-3′. Transfection was performed using Lipofectamine RNAiMAX (Invitrogen) as described previously (31). Briefly, 60 pmol of siRNA and 10 μl of Lipofectamine RNAiMAX were mixed in 1 ml of RPMI medium (10 nmol/l final siRNA concentration). After 20 min of incubation, the mixture was added to the cells and these were plated on dishes for each assay. Forty-eight hours after transfection, cells were analyzed for all experiments. The cells were seeded at a density of 2000 cells per well in 96-well plates. For constitutive expression of HOXA10, cDNA was amplified by PCR and subcloned into pcDNA 3.1 (Invitrogen). Transient transfection was carried out with the FuGENE6 Transfection Reagent (Roche Diagnostics, Indianapolis, IN). Cell growth was monitored after 1, 2 and 4 days by the 3-(4,5-dimethylthiazol-2-yl)-2,5-diphenyl tetrazolium bromide (MTT) assay (32). To evaluate cell motility, a wound healing assay was performed. Cells grown to subconfluence were scraped with a sharp edge to make a cell-free area. Cells migrating into the scraped area were observed and photographs were taken every 12 h after scraping. Modified Boyden chamber assays were performed to examine invasiveness. Cells were plated at 10 000 cells per well in RPMI 1640 medium plus 1% serum in the upper chamber of a transwell insert (8 μm pore diameter; Chemicon, Temecula, CA) coated with Matrigel. Medium containing 10% serum was added in the bottom chamber. After 1 and 2 days, cells in the upper chamber were removed by scraping, and the cells remaining on the lower surface of the insert were stained with CyQuant GR dye to assess the number of cells.

Statistical methods

Correlations between clinicopathological parameters and HOXA10 staining were analyzed by Fisher's exact test. Kaplan–Meier survival curves were constructed for HOXA10, MUC5AC, MUC6, MUC2, CD10 or CDX2-positive and -negative patients to compare survival between both groups. The differences in survival curves between groups were tested for statistical significance by the log-rank test (33). P values of <0.05 were considered statistically significant. Univariate and multivariate Cox regression was used to evaluate the associations between clinical covariates and cancer-specific mortality.

Hazard ratio and 95% confidence interval were estimated from Cox proportional hazard models. For all analyses, age was treated as a categorical variable (≤65 years of age versus >65 years of age). For final multivariable Cox regression models, all variables were included, which were moderately associated ($P < 0.05$) with cancer-specific mortality.

Results

Identification of upregulated genes in GC through microarray analysis

To identify genes with increased expression in GC, we performed microarray analysis. The gene expression profiles obtained from the two primary GC samples (W226T, W246T) and the corresponding non-neoplastic gastric mucosa samples were compared. The top 20 genes that showed higher expression in the GC samples than in the corresponding non-neoplastic gastric mucosa sample by microarray analysis are each listed in Table I. The gene showing the greatest increase in expression in both GC samples by microarray was *HOXA10*. In our previous report analyzing the *PLUNC* gene, the *HOXA10* gene had the nineth greatest increase in expression in poorly differentiated adenocarcinoma of the stomach (P208T) in the microarray analysis (9). We reported a list of the 20 genes with the greatest increase in expression in these three GC samples compared with normal stomach by SAGE analysis (5). We noted that the 20 most upregulated genes identified by microarray were quite different from those identified by SAGE, indicating that genes upregulated in GC are not always detected with SAGE. We then reviewed the expression level of *HOXA10* with our SAGE data and found that the SAGE tag sequence of *HOXA10*, CATAAAAGGG, did not appear in the W226T, W246T and P208T SAGE data. Because expression of *HOXA10* has not been investigated in GC, we therefore decided to analyze it.

Messenger RNA expression of HOXA10 in systemic normal tissues and GC tissues

Quantitative RT–PCR was performed to investigate the specificity of *HOXA10* expression in 16 normal organs. As shown in Figure 1A, *HOXA10* expression was clearly detected in normal skeletal muscle and to a lesser extent in uterine endometrium, kidney and large intestine. The expression of *HOXA10* was detected at low levels, or not at all, in other normal organs, including stomach tissue. These results are consistent with those in a previous report (18). Next, we analyzed the expression of *HOXA10* in 38 GC tissue samples and 38 corresponding non-neoplastic mucosa samples by quantitative RT–PCR. Of the 38 GC cases, expression of *HOXA10* was upregulated in 27 (71%) (Figure 1B). Messenger RNA expression levels of *HOXA10* showed no correlations with T grade (depth of tumor invasion), N grade (degree of lymph node metastasis) or the tumor stage.

Immunohistochemical analysis of HOXA10 in GC and its correlation with clinicopathological parameters

To test the specificity of the anti-HOXA10 antibody, western blotting of lysates from nine GC cell lines was carried out (Figure 2A). The anti-HOXA10 antibody detected a single band of ~41 kD on western blots of MKN-45, MKN-74, TMK-1, HSC-39 and HSC-57 cell extracts. Uterus tissue was used as a positive control of HOXA10 expression. Using this antibody, we performed immunostaining of HOXA10 in 749 GC and corresponding non-neoplastic gastric mucosa samples (Figure 1). HOXA10 expression was detected in 221 of the 749 GCs (30%) and was found in the nucleus of both early GC and advanced GC. Histologically, expression of HOXA10 was observed more frequently in the differentiated type of GC than in the undifferentiated GC ($P < 0.0001$) (Table II). In non-neoplastic gastric mucosa, HOXA10 was scarcely expressed in normal gastric mucosa, whereas it was often observed in the nucleus of intestinal metaplasia (Figure 1). Next, we analyzed the relationship between HOXA10 expression and clinicopathological characteristics. HOXA10 staining showed a significant inverse correlation with the depth of invasion ($P < 0.0001$). There was no significant association between HOXA10 staining and other parameters (age, sex, N grade, M grade or stage).

Association of HOXA10 expression with the intestinal mucin phenotype of GC

We investigated the association between HOXA10 expression and various markers determining the gastric/intestinal mucin phenotypes. Out of the 749 cases examined, each molecule was detected in 437

Table I. The 20 most upregulated genes in both early and advanced GC by microarray analysis

Early GC				Advanced GC			
Symbol	Intensity		Fold	Symbol	Intensity		Fold
	W226T[a]	Non-neoplastic mucosa			W246T[b]	Non-neoplastic mucosa	
LOC339751	6514	7	931	*FGFR2*	25747	25	1030
SLC19A3	6398	17	376	*NOX1*	2765	3	922
HOXA13	2619	9	291	*IMP-3*	5772	11	525
C14orf105	1104	5	221	*HOXA10*	6255	16	391
ADH4	41 503	213	195	*TMEM16C*	1840	5	368
HOXA10	2789	15	186	*FLJ21545*	3756	13	289
LEFTY1	34 166	249	137	*KCNJ3*	5488	29	189
ZIC2	400	4	100	*CaMKIIN alpha*	1928	12	161
SPRR1A	1083	12	90	*FLJ38736*	3732	29	129
CPS1	92 949	1093	85	*NTS*	17 320	141	123
CST1	3014	36	84	*PPL8*	615	5	123
LOC136288	128	2	64	*PCLO*	1148	10	115
FLJ12971	256	4	64	*CHM*	111	1	111
FLJ42567	1952	32	61	*FLJ42567*	3498	33	106
LOC338759	175	3	58	*MGC32871*	26 808	271	99
LOC196264	172	3	57	*CDX1*	9581	97	98
NYD-SP20	165	3	55	*IMAGE:4806358*	22 819	235	97
ADH6	4558	86	53	*MGC48998*	2287	24	95
CaMKIIN alpha	612	12	51	*TFF3*	45 055	502	90
CEACAM7	306	6	51	*AFP*	9018	104	87

[a]W226T: 59-year-old man, T1N0M0, stage I, well-differentiated adenocarcinoma.
[b]W246T: 44-year-old man, T2N2M0, stage III, well-differentiated adenocarcinoma.

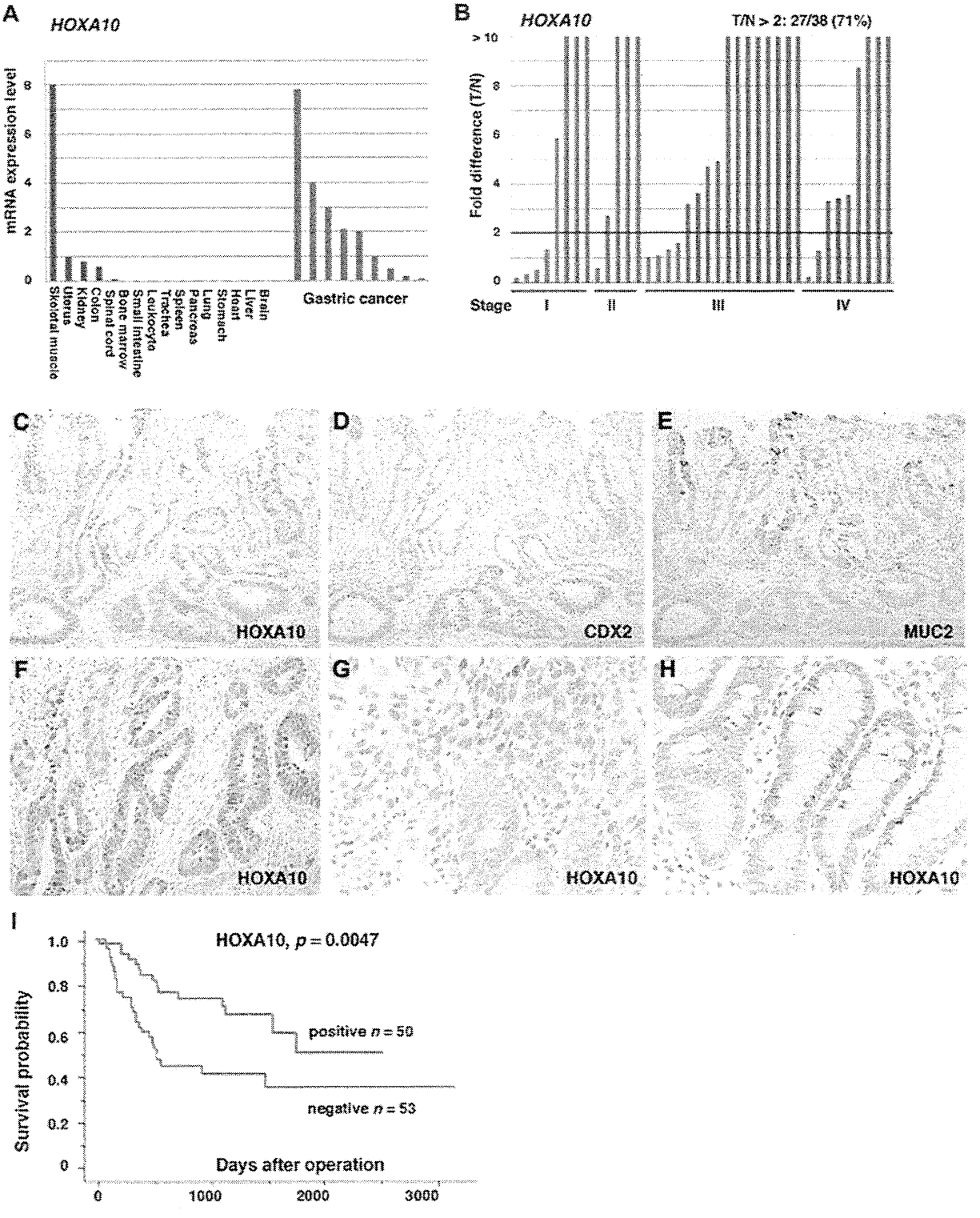

Fig. 1. Quantitative RT–PCR analysis of *HOXA10* in systemic normal tissues, GC tissues and corresponding non-neoplastic mucosa. (**A**) Clear *HOXA10* expression is present in normal skeletal muscle, uterus, kidney and colon. The units are arbitrary. (**B**) Fold-change indicates the ratio of *HOXA10* mRNA level in GC (T) to that in the corresponding non-neoplastic mucosa (N). Expression of *HOXA10* was upregulated (T/N <2) in 27 (71%) of 38 GC cases. Immunohistochemical staining of HOXA10, CDX2 and MUC2 in GC and intestinal metaplasia (**C–H**), and the relationship between HOXA10 expression and patient prognosis (**I**). HOXA10 was detected in the nucleus of both differentiated (C, F) and undifferentiated GC (G) but not in non-cancerous epithelium, except for intestinal metaplasia (H). The prognosis of patients with positive HOXA10 expression was significantly better than in the negative cases (I) ($P = 0.0047$, log-rank test). mRNA, messenger RNA.

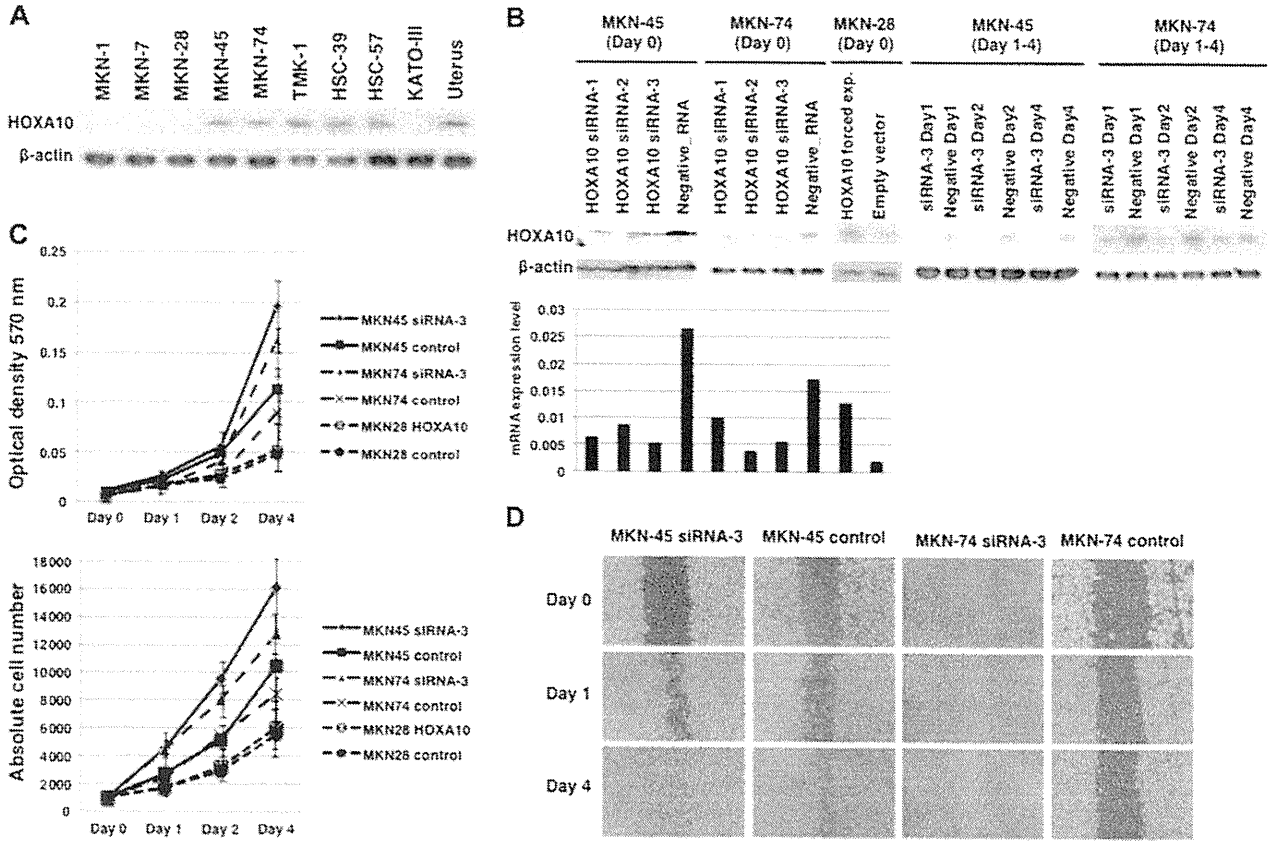

Fig. 2. Effect of *HOXA10* upregulation and downregulation on cell growth and cell motility. The anti-HOXA10 antibody detected an ~41 kD band on western blots of MKN-45, MKN-74, TMK-1, HSC-39 and HSC-57 cell extracts. Uterus tissue was used as a positive control of HOXA10 expression (**A**). Western blotting and quantitative RT–PCR analysis of HOXA10 expression in MKN-45 and MKN-74 cell lines with *HOXA10* siRNA or control scrambled siRNA transfection (Day 0–4), and MKN-28 cell line transfected with *HOXA10* cDNA or empty vector (Day 0) (**B**). To investigate the possible involvement of HOXA10 on cell growth, an 3-(4,5-dimethylthiazole-2-yl)-2,5-diphenyl tetrazolium bromide assay was performed on the fourth day after siRNA or *HOXA10* expression vector transfection (**C**). Both HOXA10 siRNA-transfected MKN-45 and MKN-74 cells showed significantly increased viability relative to control scrambled siRNA-transfected cells. Next, effects of HOXA10 expression on migration potency were determined using a wound healing assay (**D**). Both HOXA10 siRNA-transfected MKN-45 and MKN-74 cells migrating into the scratched area were significantly more than negative control cells.

(58%) cases for MUC5AC, 63 (8%) cases for MUC6, 179 (24%) cases for MUC2 and 70 (9%) cases for CD10. The 749 GC cases were classified into four phenotypes: 297 (40%) were the gastric phenotype, 172 (23%) were the gastric and intestinal mixed phenotype, 130 (17%) were the intestinal phenotype and 150 (20%) were the unclassified phenotype. Positive expression of HOXA10 was significantly more frequent in MUC2-positive cases than MUC2-negative cases ($P < 0.0001$) (Figure 1 and Table III). HOXA10 expression occurred more frequently in the intestinal phenotype and the gastric and intestinal mixed phenotype than in the gastric phenotype and the unclassified phenotype ($P = 0.0004$). On the other hand, CDX2 was detected in 195 of the 749 (26%) cases, and positive expression of HOXA10 was significantly more frequent in CDX2-positive cases than CDX2-negative cases ($P = 0.0003$) (Figure 1 and Table III). The other molecules were detected in 245 (33%) cases for β-catenin, 99 (13%) cases for EGFR and 257 (34%) cases for p53. There was no clear relationship between expression of HOXA10 and these markers.

Relationship between expression of HOXA10 in GC and patient prognosis

We also examined the relationship between survival and expression of HOXA10, CDX2 and mucins (MUC5AC, MUC6, MUC2 and CD10) in 103 GCs. The prognosis of patients with positive HOXA10 expression was significantly better than in the negative cases (Figure 1I) ($P = 0.0047$, log-rank test). The expression of the other molecules had no significant effect on the prognosis of patients (CDX2, $P = 0.1426$; MUC5AC, $P = 0.3936$; MUC6, $P = 0.9835$; MUC2, $P = 0.4996$; CD10, $P = 0.27$). In order to evaluate the potential for HOXA10 expression as a prognostic classifier, both univariate and multivariate Cox proportional hazards analyses were used to further evaluate the association of HOXA10 expression with cancer-specific mortality (Table IV). In univariate analysis, negative expression of HOXA10 (hazard ratio, 0.41; 95% confidence interval, 0.22–0.78; $P = 0.006$) and the TNM stage (hazard ratio, 6.13; 95% confidence interval, 2.84–13.3; $P < 0.0001$) was associated with survival. In the multivariate model, negative expression of HOXA10 expression and TNM stage was independent predictors of survival in patients with GC (Table IV).

Effect of HOXA10 upregulation and downregulation on cell growth, cell motility and invasive activity

HOXA10 staining showed a significant inverse correlation with the depth of invasion, suggesting that HOXA10 may be associated with tumor progression. However, the biological significance of HOXA10 in GC has not been studied. To investigate the possible involvement of HOXA10 on cell growth, an MTT assay was performed on the fourth day after *HOXA10* siRNA or control scrambled siRNA transfection in the MKN-45 and MKN-74 cell lines and MKN-28 cell line transfected with HOXA10 expression vector (pcDNA-HOXA10) or empty vector.

Table II. Relation between HOXA10 expression and clinicopathological parameters in 749 cases of GC

Factor	HOXA10 expression		*P* value
	Positive (n = 221)	Negative (n = 528)	
Age			
≤65 years (n = 359)	95 (26%)	264	NS
>65 years (n = 390)	126 (32%)	264	
Sex			
Male (n = 480)	137 (29%)	343	NS
Female (n = 269)	84 (31%)	185	
T grade[a]			
T1/T2 (n = 608)	216 (36%)	392	<0.0001
T3/T4 (n = 141)	5 (4%)	136	
N grade[a]			
N0 (n = 433)	131 (30%)	302	NS
N1/N2/N3 (n = 316)	90 (28%)	226	
M grade[a]			
M0 (n = 742)	217 (29%)	525	NS
M1 (n = 7)	4 (57%)	3	
Stage[a]			
Stage 0/I (n = 425)	130 (31%)	295	NS
Stage II/III/IV (n = 324)	91 (28%)	233	
Histology[b]			
Differentiated (n = 429)	152 (35%)	277	<0.0001
Undifferentiated (n = 320)	69 (22%)	251	

P values were calculated by Fisher's exact test. NS, not significant.
[a]Tumor stage was classified according to the criteria of the International Union Against Cancer TNM classification of malignant tumors.
[b]Histology was determined according to the Japanese Classification of Gastric Cancer.

Table III. Relation between HOXA10 expression and various molecules including mucin-related markers in 749 cases of GC

Molecule	HOXA10 expression		*P* value
	Positive (221)	Negative (528)	
MUC5AC			
Positive	140 (32%)	297	NS
Negative	81 (26%)	231	
MUC6			
Positive	22 (35%)	41	NS
Negative	199 (29%)	487	
MUC2			
Positive	79 (44%)	100	<0.0001
Negative	142 (25%)	428	
CD10			
Positive	17 (24%)	53	NS
Negative	204 (30%)	485	
CDX2			
Positive	78 (40%)	117	0.0003
Negative	143 (26%)	411	
β-catenin			
Positive	69 (28%)	176	NS
Negative	152 (30%)	352	
EGFR			
Positive	32 (32%)	67	NS
Negative	189 (29%)	461	
p53			
Positive	79 (31%)	178	NS
Negative	142 (29%)	350	

P values were calculated by Fisher's exact test. EGFR, epidermal growth factor receptor; NS, not significant.

At first, we checked the upregulation or downregulation of HOXA10 from day 0 to day 4, using western blotting or quantitative RT–PCR analysis (Figure 2B). Both HOXA10 siRNA-transfected MKN-45 and

Table IV. Univariate and multivariate Cox regression analysis of HOXA10 expression and overall survival in 134 cases of GC

Factor	Univariate analysis		Multivariate analysis	
	HR (95% CI)	*P* value	HR (95% CI)	*P* value
Age				
≤65 years	1 (Reference)	0.15		
>65 years	1.82 (0.81–4.12)			
Sex				
Female	1 (Reference)	0.29		
Male	1.39 (0.75–2.58)			
HOXA10				
Negative	1 (Reference)	0.006	1 (Reference)	0.0044
Positive	0.41 (0.22–0.78)		0.39 (0.21–0.75)	
CDX2				
Negative	1 (Reference)	0.15		
Positive	0.58 (0.28–1.21)			
MUC5AC				
Negative	1 (Reference)	0.39		
Positive	0.76 (0.41–1.42)			
MUC6				
Negative	1 (Reference)	0.98		
Positive	1.01 (0.36–2.83)			
MUC2				
Negative	1 (Reference)	0.51		
Positive	0.77 (0.35–1.66)			
CD10				
Negative	1 (Reference)	0.27		
Positive	1.54 (0.71–3.32)			
TNM stage[a]				
Stage 0/I	1 (Reference)	< 0.0001	1 (Reference)	0.0044
Stage II/III/IV	6.13 (2.84–13.3)		6.45 (2.94–14.1)	
Histology[b]				
Differentiated	1 (Reference)	0.29		
Undifferentiated	1.41 (0.75–2.63)			

CI, confidence interval; HR, hazard ratio.
[a]TNM stage was classified according to the criteria of the International Union Against Cancer TNM classification of malignant tumors.
[b]Histological type was determined according to the Japanese Classification of Gastric Cancer.

MKN-74 cells showed significantly increased viability relative to negative control cells, whereas cell viability of pcDNA-HOXA10 was not different from those of a negative control vector (Figure 2C). Next, effects of HOXA10 expression on migration potency were determined using a wound healing assay. Both HOXA10 siRNA-transfected MKN-45 and MKN-74 cells migrating into the scratched area were significantly more than negative control cells (Figure 2D), whereas cell motility of pcDNA-HOXA10 was not different from those of a negative control vector (data not shown). In addition, a transwell invasion assay was performed in the MKN-45 and MKN-74 cell lines to determine the possible role of HOXA10 in the invasiveness of GC cells. Invasion ability was not significantly different between HOXA10 knockdown GC cells and control GC cells (data not shown). These results indicate that HOXA10 inhibits cell growth and cell motility but not invasion in GC cells.

Discussion

In the present study, we studied the gene expression profile using microarray data of GC samples that were previously analyzed by SAGE (5) and identified that the *HOXA10* gene was upregulated in all samples. Quantitative RT–PCR in 38 GC samples revealed that *HOXA10* was overexpressed in >70% of GCs. Because upregulation of HOXA10 was identified by microarray and quantitative RT–PCR analysis of bulk GC tissues, immunohistochemistry was required to determine whether cancer cells truly express HOXA10. Immunohistochemical analysis revealed that HOXA10-positive cancer cells were detected in 221 (30%) of the 749 GC cases. HOXA10 was frequently

expressed in MUC2-positive GC cases, and HOXA10 expression was observed at high levels in GC with intestinal mucin phenotype. Ectopic CDX2 expression plays an important role in the development of GC with intestinal phenotype (34,35). Here, we also showed that HOXA10 expression was correlated with CDX2 expression in GC tissue. A previous report indicated that overexpression of CDX2 with the N-terminal transactivation domain upregulated HOXA10 gene expression in murine bone marrow progenitors (19). Taken together, expression of HOXA10, in addition to CDX2, may be a key factor mediating the development of GC with the intestinal mucin phenotype.

In non-neoplastic gastric mucosa, HOXA10 was scarcely expressed in normal gastric mucosa. However, we often observed nuclear accumulation of HOXA10 in intestinal metaplasia. The findings that HOXA10 expression is observed in intestinal metaplasia as well as in GC with the intestinal phenotype imply that this change occurs at an early stage of stomach carcinogenesis. Aberrations of DNA methylation are now believed to be an important epigenetic alteration occurring early in many cancers (36). In addition, it has been reported that there is a relationship between aberrant methylation of *HOXA10* and its protein expression in ovarian cancer and endometrial cancer (18,37). We speculated that aberrant promoter hypomethylation of the *HOXA10* gene leads to high expression of HOXA10 in GC.

In immunohistochemical analysis, there was a significant inverse correlation between HOXA10 expression and tumor progression. In addition, the prognosis of patients with positive HOXA10 expression was significantly better than that of negative cases. The previous reports showed that enforced expression of HOXA10 in endometrial carcinoma cells inhibited invasive behavior through downregulating Snail expression and inducing E-cadherin expression (18) and that increased HOXA10 in breast cancer cells regulated p53 expression toward reduction of invasiveness (38). HOXA10 was reported to bind to the *p21* promoter and activate *p21* transcription, resulting in cell cycle arrest and differentiation in differentiating myelomonocytic cells (15). Furthermore, Sugimoto *et al.* (39) reported that the expression of HOXA10 has an important role in apoptosis induction of chronic myelogenous leukemia cells treated with tyrosine kinase inhibitors. In the present study, knockdown of HOXA10 by siRNA had an effect on cell growth and cell motility in the GC cell line but not on cell invasion. Furthermore, we observed a higher expression of HOXA10 in the differentiated type of GC compared with the undifferentiated type. This may reflect a loss of ability to express this protein along with a decrease in histological differentiation in neoplastic cells. Once malignant formation is completed, HOXA10 might deregulate the progression of GC. It is possible that loss of *HOXA10* expression could lead to tumor progression by promoting epithelial–mesenchymal transition (18). There was no clear relationship between expression of HOXA10 and β-catenin, EGFR and p53. Further studies should be performed in the near future to elucidate the tissue specificity of the detailed pathways involving HOXA10.

In the present study, we compared gene expression profiles of GC samples analyzed by microarray analysis and SAGE. The 20 genes showing the greatest increase in expression on the microarrays were quite different from those obtained with the SAGE library. Investigation of the difference between microarray analysis and SAGE is beyond the scope of the present study and will be described elsewhere.

In summary, we demonstrated that HOXA10 is frequently upregulated in GC with the intestinal mucin phenotype and HOXA10 expression correlates with favorable survival in patients with GC. HOXA10 expression may be a key factor mediating the biological behavior of the intestinal phenotype of GC.

Funding

This work was supported, in part, by grants-in-aid for Cancer Research from the Ministry of Education, Culture, Science, Sports and Technology of Japan and in part by a grant-in-aid for the Third Comprehensive 10-year Strategy for Cancer Control and for Cancer Research from the Ministry of Health, Labour and Welfare of Japan.

Acknowledgements

We thank Mr Shinichi Norimura for his excellent technical assistance and advice. This work was carried out with the kind cooperation of the Research Center for Molecular Medicine, Faculty of Medicine, Hiroshima University. We also thank the Analysis Center of Life Science, Hiroshima University, for the use of their facilities.

Conflict of Interest Statement: None declared.

References

1. Yasui,W. *et al.* (2005) Recent advances in molecular pathobiology of gastric carcinoma. In Kaminishi,M., Takubo,K. and Mafune,K. (eds) *The Diversity of Gastric Carcinoma: Pathogenesis, Diagnosis and Therapy*. Springer, Tokyo, Japan, 51–71.
2. Yasui,W. *et al.* (2004) Search for new biomarkers of gastric cancer through serial analysis of gene expression and its clinical implications. *Cancer Sci.*, **95**, 385–392.
3. Lockhart,D.J. *et al.* (1996) Expression monitoring by hybridization to high-density oligonucleotide arrays. *Nat. Biotechnol.*, **14**, 1675–1680.
4. Velculescu,V.E. *et al.* (1995) Serial analysis of gene expression. *Science*, **270**, 484–487.
5. Oue,N. *et al.* (2004) Gene expression profile of gastric carcinoma: identification of genes and tags potentially involved in invasion, metastasis, and carcinogenesis by serial analysis of gene expression. *Cancer Res.*, **64**, 2397–2405.
6. Ferguson,D.A. *et al.* (2005) Selective identification of secreted and transmembrane breast cancer markers using *Escherichia coli* ampicillin secretion trap. *Cancer Res.*, **65**, 8209–8217.
7. Oue,N. *et al.* (2005) Expression and localization of Reg IV in human neoplastic and non-neoplastic tissues: Reg IV expression is associated with intestinal and neuroendocrine differentiation in gastric adenocarcinoma. *J. Pathol.*, **207**, 185–198.
8. Sentani,K. *et al.* (2008) Immunohistochemical staining of Reg IV and claudin-18 is useful in the diagnosis of gastrointestinal signet ring cell carcinoma. *Am. J. Surg. Pathol.*, **32**, 1182–1189.
9. Sentani,K. *et al.* (2008) Gene expression profiling with microarray and SAGE identifies PLUNC as a marker for hepatoid adenocarcinoma of the stomach. *Mod. Pathol.*, **21**, 464–475.
10. Sentani,K. *et al.* (2010) Upregulation of connexin 30 in intestinal phenotype gastric cancer and its reduction during tumor progression. *Pathobiology*, **77**, 241–248.
11. Anami,K. *et al.* (2010) Search for transmembrane protein in gastric cancer by the *Escherichia coli* ampicillin secretion trap: expression of DSC2 in gastric cancer with intestinal phenotype. *J. Pathol.*, **221**, 275–284.
12. McGinnis,W. *et al.* (1992) Homeobox genes and axial patterning. *Cell*, **68**, 283–302.
13. Chen,K.N. *et al.* (2005) Expression of 11 HOX genes is deregulated in esophageal squamous cell carcinoma. *Clin. Cancer Res.*, **11**, 1044–1049.
14. Lawrence,H.J. *et al.* (1992) Homeobox genes in normal hematopoiesis and leukemia. *Blood*, **80**, 2445–2453.
15. Bromleigh,V.C. *et al.* (2000) p21 is a transcriptional target of HOXA10 in differentiating myelomonocytic cells. *Genes Dev.*, **14**, 2581–2586.
16. SlanyR.K. (2005) When epigenetics kills: MLL fusion proteins in leukemia. *Hematol. Oncol.*, **23**, 1–9.
17. Sarno,J.L. *et al.* (2005) HOXA10, Pbx2, and Meis1 protein expression in the human endometrium: formation of multimeric complexes on HOXA10 target genes. *J. Clin. Endocrinol. Metab.*, **90**, 522–528.
18. Yoshida,H. *et al.* (2006) Deregulation of the HOXA10 homeobox gene in endometrial carcinoma: role in epithelial-mesenchymal transition. *Cancer Res.*, **66**, 889–897.
19. Rawat,V.P. *et al.* (2008) Overexpression of CDX2 perturbs HOX gene expression in murine progenitors depending on its N-terminal domain and is closely correlated with deregulated HOX gene expression in human acute myeloid leukemia. *Blood*, **111**, 309–319.
20. Japanese Gastric Cancer Association. (2011) Japanese classification of gastric carcinoma: 3rd English edition. *Gastric Cancer*, **14**, 101–112.
21. Nishigaki,M. *et al.* (2005) Discovery of aberrant expression of R-RAS by cancer-linked DNA hypomethylation in gastric cancer using microarrays. *Cancer Res.*, **65**, 2115–2124.
22. Gibson,U.E. *et al.* (1996) A novel method for real time quantitative RT-PCR. *Genome Res.*, **6**, 995–1001.
23. Kondo,T. *et al.* (2004) Expression of POT1 is associated with tumor stage and telomere length in gastric carcinoma. *Cancer Res.*, **64**, 523–529.

24. Yasui,W. *et al.* (1993) Increased expression of p.34cdc2 and its kinase activity in human gastric and colonic carcinomas. *Int. J. Cancer*, **53**, 36–41.
25. Mizoshita,T. *et al.* (2003) Expression of Cdx2 and the phenotype of advanced gastric cancers: relationship with prognosis. *J. Cancer Res. Clin. Oncol.*, **129**, 727–734.
26. Ochiai,A. *et al.* (1985) Growth-promoting effect of gastrin on human gastric carcinoma cell line TMK-1. *Jpn. J. Cancer Res.*, **76**, 1064–1071.
27. Hojo,H. *et al.* (1977) Establishment of cultured cell lines of human stomach cancer origin and their morphological characteristics. *Niigata Igakkai Zasshi*, **91**, 737–763.
28. Motoyama,T. *et al.* (1986) Comparison of seven cell lines derived from human gastric carcinomas. *Acta Pathol. Jpn.*, **36**, 65–83.
29. Sekiguchi,M. *et al.* (1978) Establishment of cultured cell lines derived from a human gastric carcinoma. *Jpn. J. Exp. Med.*, **48**, 61–68.
30. Yanagihara,K. *et al.* (1991) Establishment and characterization of human signet ring cell gastric carcinoma cell lines with amplification of the c-myc oncogene. *Cancer Res.*, **51**, 381–386.
31. Sakamoto,N. *et al.* (2010) Serial analysis of gene expression of esophageal squamous cell carcinoma: ADAMTS16 is upregulated in esophageal squamous cell carcinoma. *Cancer Sci.*, **101**, 1038–1044.
32. Alley,M.C. *et al.* (1988) Feasibility of drug screening with panels of human tumor cell lines using a microculture tetrazolium assay. *Cancer Res.*, **48**, 589–601.
33. Mantel,N. (1966) Evaluation of survival data and two new rank order statistics arising in its consideration. *Cancer Chemother. Rep.*, **50**, 163–170.
34. Tatematsu,M. *et al.* (2003) Stem cells and gastric cancer: role of gastric and intestinal mixed intestinal metaplasia. *Cancer Sci.*, **94**, 135–141.
35. Silberg,D.G. *et al.* (2002) Cdx2 ectopic expression induces gastric intestinal metaplasia in transgenic mice. *Gastroenterology*, **122**, 689–696.
36. Feinberg,A.P. *et al.* (2004) The history of cancer epigenetics. *Nat. Rev. Cancer*, **4**, 143–153.
37. Cheng,W. *et al.* (2010) Identification of aberrant promoter hypomethylation of HOXA10 in ovarian cancer. *J. Cancer Res. Clin. Oncol.*, **136**, 1221–1227.
38. Chu,M.C. *et al.* (2004) HOXA10 regulates p.53 expression and matrigel invasion in human breast cancer cells. *Cancer Biol. Ther.*, **3**, 568–572.
39. Sugimoto,Y. *et al.* (2008) HOXA10 expression induced by Abl kinase inhibitors enhanced apoptosis through PI3K pathway in CML cells. *Leuk. Res.*, **32**, 962–971.

Received November 3, 2011; revised February 19, 2012; accepted March 3, 2012

The Impact of Superior Mediastinal Lymph Node Metastases on Prognosis in Non-small Cell Lung Cancer Located in the Right Middle Lobe

Yukinori Sakao, MD, PhD, Sakae Okumura, MD,* Mun Mingyon, MD, PhD,* Hirofumi Uehara, MD, PhD,* Yuichi Ishikawa, MD, PhD,† and Ken Nakagawa, MD**

Background: We aimed to assess hilar and mediastinal lymph node involvement and its impact on prognosis in patients with right middle lobe lung cancer.

Methods: The records of 170 patients undergoing surgery for right middle lobe non-small cell lung cancer from 1980 to December 2007 were retrospectively examined. There were 45 patients found to have hilar or mediastinal lymph nodes metastases. This subgroup included 31 N2 patients and 14 N1 patients, and included 23 women and 22 men, whose ages ranged from 32 to 83 years (median = 61 years). The status of mediastinal, hilar, and interlobar lymph nodes was assessed according to the seventh edition of the TNM classification for lung cancer. Patient records were examined for age, gender, preoperative nodal status, surgical procedure, metastatic status of lymph nodes (distribution and numbers), tumor size, and histologic features (cell type and differentiation degree). Survival duration was defined as the interval between surgery and death from the tumor or the most recent follow-up.

Results: For N1 cases (n = 14), the most frequent metastatic site was #12m (lymph nodes adjacent to the middle lobe bronchus), which occurred in 11 cases; there was one case with metastases in #11s (lymph nodes between the upper lobe bronchus and bronchus intermedius), and no case with #11i metastases (lymph nodes between the right middle and lower lobe bronchi). The most frequent metastatic mediastinal zone was the subcarinal zone (25/31), and the superior mediastinal zone also had a high incidence of metastases (22/31). Sixteen cases had metastases to both the superior and subcarinal zones, and six cases had metastasis to superior mediastinal zone without subcarinal zone metastasis. When #11s or #11i was involved, eight of nine or five of five, respectively, were N2 cases. Univariate analyses revealed that tumor diameter, cN, status of lymph node metastases, and operative procedure (pneumonectomy) were significant prognostic factors in N2 cases. Regarding status of lymph node metastases, superior mediastinal zone metastases, both superior and inferior (subcarinal) zone metastases, and #11i were significant prognostic factors. Because #11i metastases and superior mediastinal lymph nodes metastases were highly correlated with each other (p = 0.02), two separate models were used in multivariate analyses. Superior mediastinal metastases (p = 0.03) and #11i metastases (p = 0.015) were revealed to be significant independent prognostic factors, whereas multiple-zone metastases only tended toward significance as an adverse prognostic factor (p = 0.054).

Conclusions: Superior mediastinal lymph node metastases and #11i metastases were significant adverse prognostic factors in patients with middle lobe lung cancer, and they were associated with each other.

Key Words: Middle lobe cancer, Superior mediastinal lymph node metastasis, N2, NSCLC.

(*J Thorac Oncol.* 2011;6: 494–499)

The right middle lobe is the smallest lobe in the lung, and lung cancer originating there is much less common than in the other lobes, occurring in 3.8 to 6.7% of all lung cancers.[1–4] The fact that it is less common may be a reason that there are a few reports on the prognostic factors of middle lobe lung cancer.

Lymph drainage from the middle lobe extends to both superior and inferior mediastinal lymph nodes, and previous reports have demonstrated a high incidence of metastases to both the superior and inferior mediastinal zones.[1–6] Nevertheless, there are few articles on the relationships between status of hilar and mediastinal lymph node metastases and patient prognoses.

In this retrospective study, we aimed to clarify prognostic factors in patients with middle lobe lung cancer who underwent surgery. Furthermore, we wanted to determine the association between the status of lymph node metastases and postoperative prognosis.

PATIENTS AND METHODS

This was a retrospective study. Because individual patients were not identified, our institutional review board waived the requirement for obtaining patient consent and approved this study. Between 1980 and December 2007, 170 patients underwent surgical resection at the Cancer Institute

Departments of *Thoracic Surgical Oncology and †Pathology, Japanese Foundation for Cancer Research, Cancer Institute Hospital, Tokyo, Japan.

Disclosure: The authors declare no conflicts of interest.

Address for correspondence: Yukinori Sakao, MD, PhD, Department of Thoracic Surgical Oncology, Japanese Foundation for Cancer Research, Cancer Institute Hospital, 3-10-6, Ariake, Koto-ku, Tokyo 135-8550, Japan. E-mail: yukinori.sakao@jfcr.or.jp

ISSN: 1556-0864/11/0603-0494

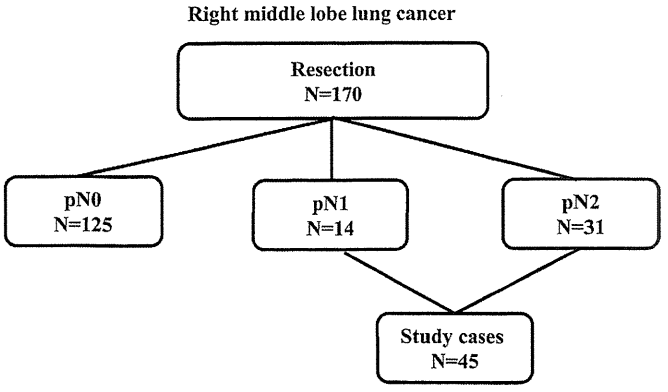

FIGURE 1. Study group subdivisions. Between 1980 and December 2007, 170 patients underwent surgical resections for right middle lobe lung cancer at the Cancer Institute Hospital. There were 14 N1 cases and 31 N2 cases evaluated.

Hospital for primary lung cancer originating in the right middle lobe. Among these patients, 45 were diagnosed with N1 or N2 disease after lung resection and hilar and mediastinal node dissections (Figure 1). The extent of lymph node dissection was not affected by a suspicion of N1 disease. We have routinely performed nearly the same dissection (ND2a).

All the 45 study patients were confirmed for their prognoses. The primary surgical procedure for lymph node dissection, such as hilar and mediastinal nodal dissection, was established in Japan in the late 1970s. In our institute, the extent of lymph node dissection conducted recently is nearly the same as that during the 1980s. Some cases had sampling due to disorders such as cardiac or pulmonary, and these cases were excluded from this study. The resected lymph nodes were separated according to the map[7] in the operating room by the surgeons. Station 10 nodes dissected in middle lobe cancer were adjacent to the inferior parts of the main bronchus, and these nodes were included in the subcarinal zone according to the new TNM. [7] The other station 10 nodes, which were adjacent to the upper parts of the main bronchus, were not routinely dissected, and this area is difficult to dissect without an upper lobectomy.

This subgroup included 31 N2 patients and 14 N1 patients, and included 23 women and 22 men, whose ages ranged from 32 to 83 years (median = 61 years, Table 1). For all patients, preoperative staging was performed using chest computed tomography (CT), abdominal CT or ultrasonography, brain CT or magnetic resonance imaging, and bone scans. Clinical mediastinal and hilar lymph node status was assessed as positive if the chest CT showed that the short axis of a node was more than 1.0 cm. CT scans have been used for evaluating lung cancer staging in our institute since 1980. Of course, CT imaging quality is different when comparing that in the 1980s with that in the 2000s. Nevertheless, this study focused on pathological N status of middle lobe lung cancer, and the quality of pathological examinations was nearly the same during the study period. We excluded those patients who had induction therapy because it seemed to be difficult to evaluate their pathological node status.

TABLE 1. Patient Characteristics

Age (yr)	32–83, median: 61
Gender (male/female)	22/23
c-N	
N0/N1/N2	23/14/8
c-T	
T1/T2/T3/T4	17/24/3/1
p-N	
N1/N2	14/31
Histologic type	
Adenocarcinoma/others	35/10
Well-differentiated/others	10/35
Surgical procedure	
Lobectomy/bilobectomy/pneumonectomy	21/14/10

Bulky N2 (shortest mediastinal lymph node diameter >2 cm) patients have not been candidates for surgery in our institute. Although mediastinoscopy, 18F-fluorodeoxyglucose positron emission tomography, or endobronchial ultrasound with transbronchial needle aspiration was applied to some patients in this series, they were not used for preoperative staging. Follow-up periods ranged from 2 to 302 months (median follow-up for living patients was 86 months).

The status of mediastinal, hilar, or interlobar nodes was assessed according to the seventh edition of the TNM classification for lung cancer.[7] Mediastinal nodes were classified into the following three zones: superior, subcarinal, and inferior. N1 nodes were classified into two zones as hilar or interlobar, and peripheral. The interlobar zone was divided into three subgroups as follows: #12m, lymph nodes adjacent to the middle lobe bronchus; #11s, lymph nodes between the upper lobe bronchus and bronchus intermedius; and #11i, lymph nodes between the right middle and lower lobe bronchi. When a case had mediastinal nodal involvement of two or more zones, it was classified with multiple-zone metastases.

Patient characteristics are summarized in Table 1. Patient records were examined for age, gender, preoperative nodal status, surgical procedure, metastatic status of lymph nodes (distribution and numbers), tumor size, and histologic features (cell type and degree of differentiation).

Statistical Analysis

Survival duration was defined as the interval between surgery and death from the tumor, or the most recent follow-up. Survival rates were calculated using the Kaplan-Meier method. Univariate analyses were performed using the log-rank test, χ^2 test, and logistic regression. Multivariate analyses were performed for variables with p values less than 0.1 by univariate analysis, using the logistic regression test in StatView J 5.0 (SAS Institute Inc., Cary, NC). A p value less than 0.05 was considered significant.

RESULTS

Status of Lymph Node Metastases

In N1 cases (n = 14), the most frequent metastatic site was #12m, occurring in 11 cases, and there was one case with metastases in #11s and 0 cases with #11i metastases (Figure 2).

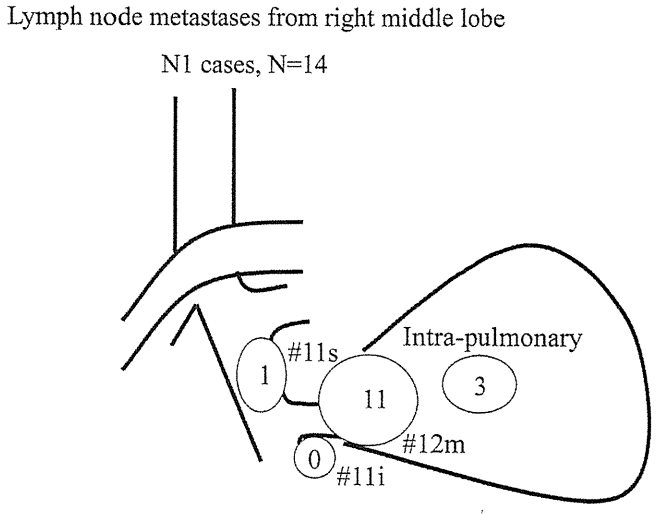

FIGURE 2. Distribution of metastatic nodes in N1 cases.

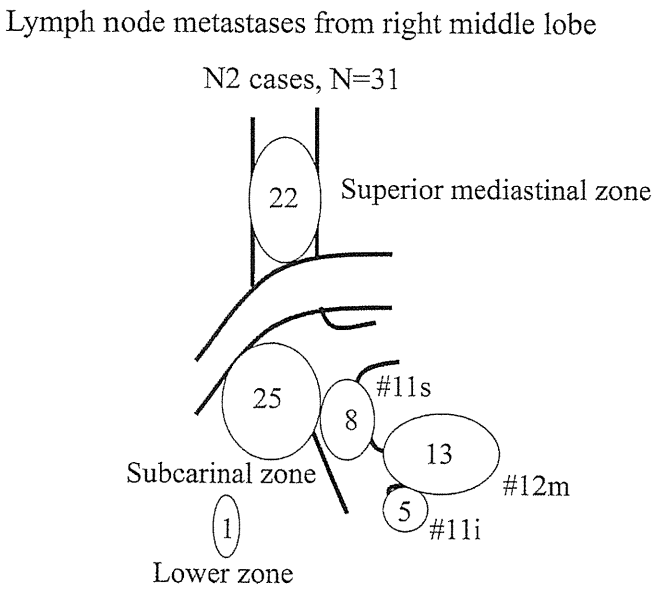

FIGURE 3. Distribution of metastatic nodes in N2 cases.

The most frequent metastatic mediastinal zone was the subcarinal zone (25/31 N2 cases). The superior zone also had a high incidence of metastases (22/31 cases). There were 16 cases with metastases in both the superior and subcarinal zones; nine cases were metastasized to the subcarinal zone without the superior mediastinal zone metastasis, and six cases were metastasized to superior the mediastinal zone without the subcarinal zone metastasis (Figure 3). When #11s was involved, eight of nine cases were N2, and when #11i was involved, all five cases were N2 (Figures 4 and 5).

Survival Rates for Patients with Nodal Involvement

The postoperative 5-year survival rate for patients with N1 was 62% and with N2 was 20% ($p = 0.02$). The postoperative 5-year survival rate was 83% for 125 N0 patients. The prognoses for N0 patients with right middle lobe cancers were not different from those of N0 patients with other involved lobes.

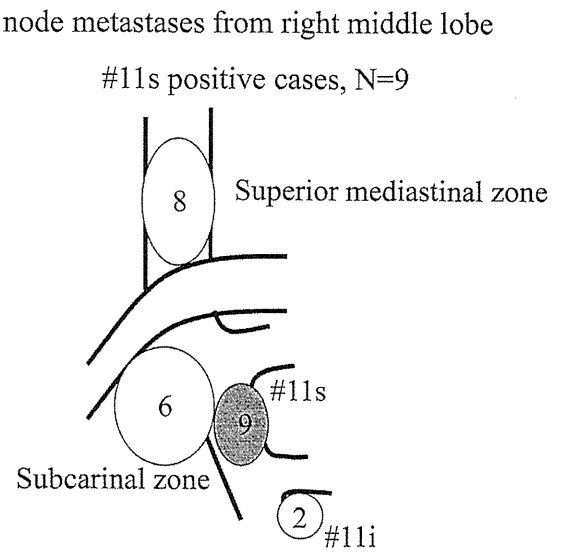

FIGURE 4. Association of #11s metastases with mediastinal zone metastases.

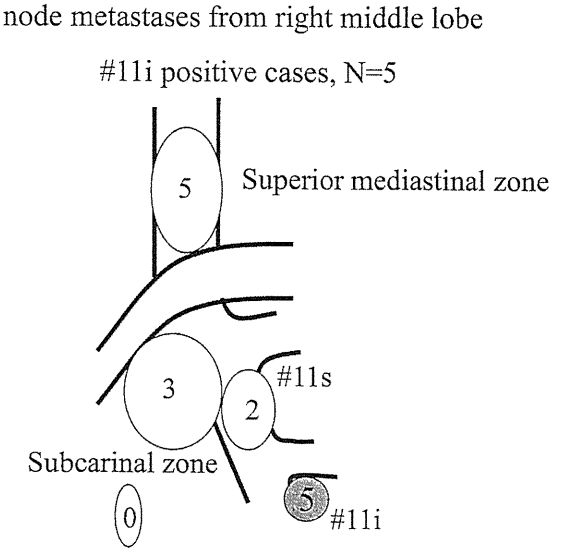

FIGURE 5. Association of #11i metastases with mediastinal zone metastases.

Prognostic Factors for N2 in the Right Middle Lobe

Univariate analyses using the variables listed in Table 2 showed that diameter, cN1–2/cN0, status of lymph node metastases, and operative procedure (pneumonectomy) were significant prognostic factors. Nevertheless, there was no difference in prognoses between lobectomy and bilobectomy. Regarding specific prognostic lymph node metastases, superior mediastinal zone metastases, both superior and subcarinal and interlobar #11i metastases were significant prognostic factors. Inferior mediastinal zone metastases, and #12m and

TABLE 2. Prognostic Factors for Patients with N2: Univariate Analysis

Variables	Cases	5-yr Survival (%)	*p*
Gender			
Male/female	14/17	17.8/22.0	0.95
Age			
<70 yr/70 yr or older	22/9	21.7/16.0	0.37
Diameter (14–65 mm, mean: 35 mm)			
<35 mm/35 mm or larger	16/15	36.5/6.8	0.02
cN			
cN1–2/cN0	15/16	8.0/33.7	0.042
cN0–1/cN2	23/8	23.3/12.5	0.24
Adenocarcinoma/others	26/5	25.2/0	0.1
Well differentiated/others	6/25	16.7/21.5	0.81
Pleural involvement yes/no	15/16	21.8/17.3	0.57
Status of lymph node metastases			
Superior mediastinal zone yes/no	22/9	6.4/50.8	0.005
Inferior mediastinal zone yes/no	25/6	21.4/16.7	0.61
#12m yes/no	13/18	24.7/18.3	0.92
#11s yes/no	8/23	14.3/21.9	0.14
#11i yes/no	5/26	0/23.6	0.02
Both superior and inferior zones			
Multiple zones/single zone	16/15	0/36.4	0.01
Operative procedure			
Pneumonectomy vs. others	7/24	0/25.8	0.009
Lobectomy vs. bilobectomy	16/8	23.6/29.2	0.61
Period			
Before 1995 vs. from and after 1995	15/16	13.3/28.4	0.28

#12m, lymph nodes adjacent to middle lobe bronchus; #11s, lymph nodes between the upper lobe bronchus and bronchus intermedius; #11i, lymph nodes between the right middle and lower lobe bronchi.

TABLE 3. Prognostic Factors for Patients with N2: Multivariate Analysis

Variables	Odds Ratio	95% CI	*p*
Model 1			
Diameter	1.04	0.99–1.08	0.054
cN			
cN1–2/cN0	1.87	0.71–4.95	0.21
Status of lymph node metastases			
Superior mediastinal zone	5.08	1.20–21.8	0.03
Multiple zones	1.42	0.51–3.96	0.50
Operative procedure			
Pneumonectomy	1.13	0.30–4.34	0.88
Model 2			
Diameter	1.03	0.99–1.06	0.17
cN			
cN1–2/cN0	1.38	0.54–3.52	0.51
Status of lymph node metastases			
#11i	4.80	1.34–17.0	0.015
Multiple zones	2.80	0.98–7.96	0.054
Operative procedure			
Pneumonectomy	2.32	0.62–10.0	0.20

#11i, lymph nodes between the right middle and lower lobe bronchi.

#11s metastases were not significant. There was no difference in prognoses between the patients before 1995 and patients from 1996 and after (5-year survivals of 13.3% and 28.4%; $p = 0.28$).

Significant variables by univariate analyses were analyzed by multivariate analyses (Table 3, models 1 and 2). Because #11i metastases and superior mediastinal lymph nodes metastases were highly correlated with each other ($p = 0.02$), two separate models were used for multivariate analyses. In model 1, superior mediastinal metastases were revealed to be a significant independent prognostic factor ($p = 0.03$). In model 2, #11i metastases were revealed to be a significant independent prognostic factor ($p = 0.015$), whereas multiple zone metastases only tended toward significance as an adverse prognostic factor ($p = 0.054$).

Survival Rate According to Prognostic N2 Factors

N2 patients were categorized according to whether they had significant prognostic factors determined from multivariate analyses, including superior mediastinal lymph nodes metastases, #11i metastases, or multiple mediastinal metastatic zones.

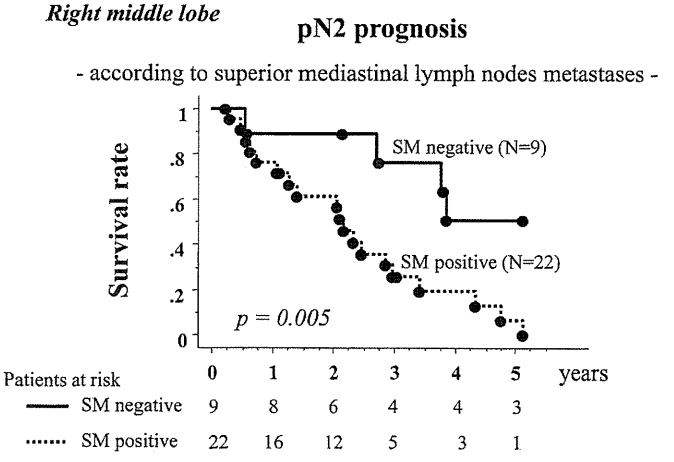

FIGURE 6. Postoperative survival according to superior mediastinal nodal involvement.

The 5-year survival rate was 50.8% in patients without superior mediastinal lymph nodes metastases, whereas it was 6.4% in patients with superior mediastinal lymph node metastases ($p = 0.005$, Figure 6). The 5-year survival rate was 23.6% in patients without #11i lymph node metastases, whereas there were no long-term survivors (dead within 3 years) in patients with #11i lymph node metastases ($p = 0.008$, Figure 7). Furthermore, the 3-year and 5-year survival rates were 58.2% and 36.4% in patients with single-zone mediastinal lymph node metastases, whereas they were 29.6% and 0% in patients with multiple-zone mediastinal lymph node metastases ($p = 0.01$), respectively. Nevertheless, by multivariate analysis, superior mediastinal lymph

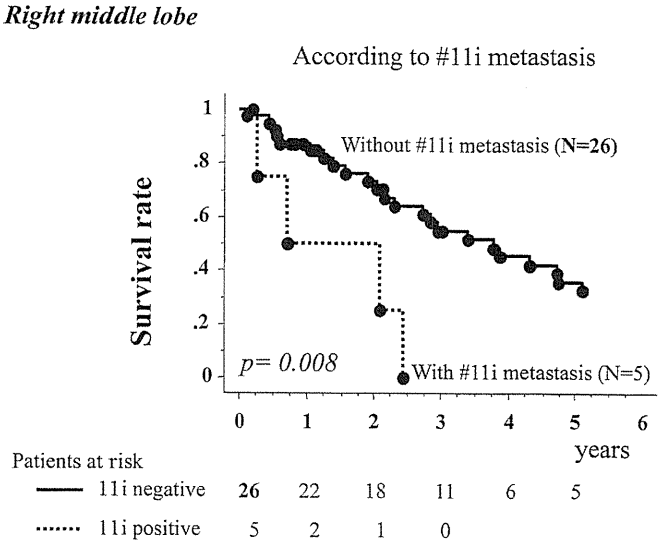

FIGURE 7. Postoperative survival according to #11i nodal involvement.

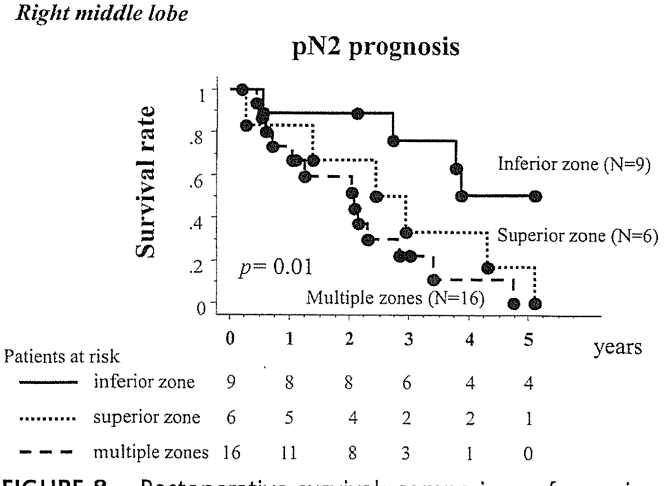

FIGURE 8. Postoperative survival: comparison of superior mediastinal nodal involvement with multiple-zone metastases.

node metastases were revealed to be a stronger prognostic factor than multiple metastatic zones (Figure 8).

DISCUSSION

There have been many reports on the prognostic impact of metastasis to specific mediastinal zones, especially lung cancer in the upper or lower lobes. For patients with lung cancer with tumor originating in the upper lobe or division, the frequency of subcarinal lymph node metastases has been reported to range from 3 to 5%, with the 5-year survival rates ranging from 9 to 18%.[8–10] The frequency of superior mediastinal lymph node metastases has been reported to range from 4 to 5%, with 5-year survival rates ranging from 0 to 19%.[10,11] This low-frequency mediastinal lymph node involvement was highly associated with multilevel N2, and therefore, the outcomes were poor.[10,12,13] In this study, the frequency of metastases was similar for the subcarinal and superior mediastinal zones, and the incidences in N2 patients were 80.6% and 71.0%, respectively. Thus, both superior and inferior mediastinal zones were found to be major metastatic sites, and these results are compatible with previous reports.[14]

We have revealed that metastases to the superior mediastinal lymph nodes are an important independent prognostic factor in patients with N2 middle lobe cancer. This is similar to what is seen in lower lobe cancer. Nevertheless, the incidence of skip metastasis to the superior mediastinum is very different between cancer in the middle lobe and in the lower lobe. The incidence in this study was 20% for N2 and has been reported to range from 3 to 4.5% in N2 right lower lobe cancer.[10–12] Furthermore, there was a significant difference in the 5-year survival rates for superior mediastinal involvement and inferior mediastinal involvement (6.5% and 50.8%, respectively), even for single-zone N2. When superior mediastinal lymph nodes were involved, the prognosis was almost the same as for multilevel N2 patients with middle lobe cancer.

The most frequent metastatic hilar lymph node was #12m, and most #11s and #11i metastases were found in N2 patients. In other words, metastases found in #11s or #11i indicate N2 disease (#11s: 8/9 and #11i: 5/5). Surprisingly, interlobar (lower lobe: #11i) lymph node involvement was an important adverse prognostic factor, even in N2 patients. This may be explained by the fact that there was an association between #11i metastases and superior mediastinal nodal involvement. Metastasis in #11i may be understood to be a result of mediastinal nodal involvement. That is, #11i metastasis is retrograde because of disturbed antegrade lymph drainage to the superior mediastinum from mediastinal metastases. Unfortunately, we could not find any previous reports regarding this correlation between #11i and superior mediastinal node involvement. Further investigation is needed to prove the hypothesis that #11i metastases result from superior mediastinal lymph node metastases.

In conclusion, superior mediastinal lymph node metastases and #11i metastases were significant adverse prognostic factors in patients with middle lobe lung cancer, and they were associated with each other. Furthermore, in patients with middle lobe lung cancer, #11i metastases may result from mediastinal metastases, and the impact on prognosis must be different from that of patients with cancer in other lobes.

Limitations of this study include its retrospective nature, including cases from the 1980s, a small sample number, and that routine adjuvant chemotherapy for N2 patients was started in 2006. Therefore, in this study, it was difficult to evaluate the effects on prognosis with respect to adjuvant chemotherapy.

REFERENCES

1. Vincent RG, Takita H, Lane WW, et al. Surgical therapy of lung cancer. *J Thorac Cardiovasc Surg* 1976;71:581–591.
2. Freise G, Gabler A, Liebig S. Bronchial carcinoma and long-term survival. Retrospective study of 433 patients who underwent resection. *Thorax* 1978;33:228–234.

3. Gifford JH, Waddington JKB. Review of 464 cases of carcinoma of lung treated by resection. *Br Med* 1957;30:723–730.
4. Ochsner A, Ray CJ, Acreea PW. Cancer of lung; review of experiences with 1457 cases of bronchogenic carcinoma. *Am Rev Tuberc* 1954;70:763–783.
5. Riquet M, Dupont P, Hidden G, et al. Lymphatic drainage of the middle lobe of the adult lung. *Surg Radio Anat* 1990;12:231–233.
6. Hata E, Hayakawa K, Miyamoto H, et al. Rationale for extended lymphadenectomy for lung cancer. *Thorac Surg* 1990;5:19–25.
7. Rusch VW, Asamura H, Watanabe H, et al. Members of IASLC Staging Committee. The IASLC lung cancer staging project: a proposal for a new international lymph node map in the forthcoming seventh edition of the TNM classification for lung cancer. *J Thorac Oncol* 2009;4:1043–1045.
8. Asamura H, Nakayama H, Kondo H, et al. Lobe-specific extent of systematic lymph node dissection for non-small cell lung carcinomas according to a retrospective study of metastasis and prognosis. *J Thorac Cardiovasc Surg* 1999;117:1102–1111.
9. Uehara H, Okumura S, Satoh Y, et al. Validity of omission of subcarinal lymph node dissection in patients with cancer of the right upper lobe or left upper division of the lung. *Jpn J Lung Cancer* 2008;48:266–272.
10. Okada M, Sakamoto T, Yuki T, et al. Border between N1 and N2 stations in lung carcinoma: lessons from lymph node metastatic patterns of lower lobe tumors. *J Thorac Cardiovasc Surg* 2008;129: 825–830.
11. Uehara H, Sakao Y, Mun M, et al. Prognostic value and significance of subcarinal and superior mediastinal lymph node metastasis in lower lobe tumours. *Eur J Cardiothorac Surg* 2010;38:498–502.
12. Ichinose Y, Kato H, Koike T, et al. Japanese Clinical Oncology Group. Completely resected stage IIIA non-small cell lung cancer: the significance of primary tumor location and N2 station. *J Thorac Cardiovasc Surg* 2001;122:803–808.
13. Sakao Y, Miyamoto H, Yamazaki A, et al. The prognostic significance of metastasis to the highest mediastinal lymph node in non-small cell lung cancer. *Ann Thorac Surg* 2006;81:292–297.
14. Naruke T, Tsuchiya R, Kondo H, et al. Lymph node sampling in lung cancer: how should it be done? *Eur J Cardiothorac Surg* 1999;16:S17–S24.

Published OnlineFirst on March 23, 2011; DOI:10.1158/1078-0432.CCR-11-0063

Clinical Cancer Research

Pulmonary Inflammatory Myofibroblastic Tumor Expressing a Novel Fusion, PPFIBP1 –ALK: Reappraisal of Anti-ALK Immunohistochemistry as a Tool for Novel ALK Fusion Identification

Kengo Takeuchi, Manabu Soda, Yuki Togashi, et al.

Clin Cancer Res Published OnlineFirst March 23, 2011.

Published OnlineFirst on March 23, 2011; DOI:10.1158/1078-0432.CCR-11-0063

Clinical Cancer Research

Imaging, Diagnosis, Prognosis

Pulmonary Inflammatory Myofibroblastic Tumor Expressing a Novel Fusion, PPFIBP1–ALK: Reappraisal of Anti-ALK Immunohistochemistry as a Tool for Novel ALK Fusion Identification

Kengo Takeuchi[1,2], Manabu Soda[4], Yuki Togashi[1,2], Emiko Sugawara[1,5], Satoko Hatano[1,2], Reimi Asaka[1,2], Sakae Okumura[3], Ken Nakagawa[3], Hiroyuki Mano[4,6], and Yuichi Ishikawa[2]

Abstract

Purpose: The anaplastic lymphoma kinase (ALK) inhibitor crizotinib has been used in patients with lung cancer or inflammatory myofibroblastic tumor (IMT), both types harboring ALK fusions. However, detection of some ALK fusions is problematic with conventional anti-ALK immunohistochemistry because of their low expression. By using sensitive immunohistochemistry, therefore, we reassessed "ALK-negative" IMT cases defined with conventional immunohistochemistry (approximately 50% of all examined cases).

Experimental Design: Two cases of ALK-negative IMT defined with conventional anti-ALK immunohistochemistry were further analyzed with sensitive immunohistochemistry [the intercalated antibody-enhanced polymer (iAEP) method].

Results: The two "ALK-negative" IMTs were found positive for anti-ALK immunohistochemistry with the iAEP method. 5′-rapid amplification of cDNA ends identified a novel partner of ALK fusion, protein-tyrosine phosphatase, receptor-type, F polypeptide-interacting protein-binding protein 1 (PPFIBP1) in one case. The presence of PPFIBP1–ALK fusion was confirmed with reverse transcriptase PCR, genomic PCR, and FISH. We confirmed the transforming activities of PPFIBP1–ALK with a focus formation assay and an *in vivo* tumorigenicity assay by using 3T3 fibroblasts infected with a recombinant retrovirus encoding PPFIBP1–ALK. Surprisingly, the fusion was also detected by FISH in the other case.

Conclusions: Sensitive immunohistochemical methods such as iAEP will broaden the potential value of immunohistochemistry. The current ALK positivity rate in IMT should be reassessed with a more highly sensitive method such as iAEP to accurately identify those patients who might benefit from ALK-inhibitor therapies. Novel ALK fusions are being identified in various tumors in addition to IMT, and thus a reassessment of other "ALK-negative" cancers may be required in the forthcoming era of ALK-inhibitor therapy. *Clin Cancer Res; 17(10); 1–8. ©2011 AACR.*

Introduction

Anaplastic lymphoma kinase (ALK) is a receptor tyrosine kinase that was discovered in anaplastic large cell lymphoma (ALCL) in the form of a fusion protein, NPM–ALK. (1, 2). In addition to ALCL (fused to NPM, TPM3, TPM4, ATIC, TFG, CLTC, MSN, MYH9, or ALO17; refs. 1–10), ALK has further been found to generate fusions in inflammatory myofibroblastic tumor (IMT; TPM3, TPM4, CLTC, CARS, RANBP2, ATIC, or SEC31L1; refs. 10–15), ALK-positive large B-cell lymphoma (CLTC, NPM, SEC31L1, or SQSTM1; 16–19), lung cancer (EML4 or KIF5B; refs. 20, 21), and ALK-positive histiocytosis (TPM3; ref. 22) Besides, some ALK fusions have been reported without showing histopathologic evidence: TPM4–ALK in esophageal squamous cell carcinoma (23, 24), TFG–ALK in lung adenocarcinoma (25), and EML4–ALK in colon and breast carcinomas (26). The wild-type ALK is mainly expressed in the developing nervous system, and is usually not expressed in other normal tissues (27). A fusion protein formation with a partner through chromosomal translocations is the most common mechanism of ALK overexpression and ALK kinase domain activation. These features render ALK fusion oncokinase an ideal molecular target.

Recently, the ALK inhibitor crizotinib has been used in patients with lung cancer or IMT, both types harboring ALK fusions (28, 29). The compound showed a 57% response rate in lung cancers (28), and a strong response for several months in IMT (29). Crizotinib and other ALK inhibitors

Authors' Affiliations: [1]Pathology Project for Molecular Targets; [2]Division of Pathology; and [3]Department of Thoracic Surgical Oncology, Thoracic Center, Cancer Institute Hospital, Japanese Foundation for Cancer Research, Tokyo; [4]Division of Functional Genomics, Jichi Medical University, Tochigi; [5]Department of Comprehensive Pathology, Graduate School, Tokyo Medical and Dental University; and [6]Department of Medical Genomics, Graduate School of Medicine, University of Tokyo, Tokyo, Japan

Note: Supplementary data for this article are available at Clinical Cancer Research Online (http://clincancerres.aacrjournals.org/).

Corresponding Author: Kengo Takeuchi, Pathology Project for Molecular Targets, The Cancer Institute, Japanese Foundation for Cancer Research, Tokyo 135-8550, Japan. Phone: +8133-520-0111; Fax: +8133-570-0230; E-mail: kentakeuchi-tky@umin.net

doi: 10.1158/1078-0432.CCR-11-0063

Published OnlineFirst on March 23, 2011; DOI:10.1158/1078-0432.CCR-11-0063

Translational Relevance

Anaplastic lymphoma kinase (ALK) inhibitors have become one of the most promising groups of molecularly targeted drugs. Therefore, ALK is no longer a mere research target or simply a diagnostic marker, but is directly linked to the therapeutic benefit of patients harboring the fusions.

Pathologic diagnoses for ALK fusion-positive tumors have been made reliably with anti-ALK immunohistochemistry. Since the discovery of EML4–ALK, however, an unexpected problem in anti-ALK immunohistochemistry has become apparent, that is, the inability to detect a low level of EML4–ALK expression. To overcome this, we developed the intercalated antibody-enhanced polymer immunohistochemistry, which successfully detected EML4–ALK.

In other words, this indicates that unknown ALK fusions, particularly those expressed at a low level, may wait to be discovered in "ALK-negative" tumors defined with conventional immunohistochemistry. In the forthcoming era of ALK-inhibitor therapy, "ALK-negative" tumors should be reassessed with a high sensitive immunohistochemistry and, if positive, be further examined with appropriate molecular method(s).

have thus become one of the most promising groups of molecularly targeted drugs. Therefore, the sensitive and accurate identification of ALK fusion in tumors has also become clinically relevant, because it is no longer a mere research target or simply a diagnostic marker, but is directly linked to the therapeutic benefit of patients harboring the fusions.

Identification of such ALK fusions, especially within ALCL, has been prompted by the immunohistochemical staining pattern with antibodies to ALK. In ALCL, the most common ALK fusion is NPM–ALK (comprising approximately 80% of all cases), and its immunohistochemical staining pattern is both nuclear and cytoplasmic. NPM has a nuclear localization signal in the C-terminal region, and therefore the heterodimers of wild-type NPM with NPM–ALK fusion protein are transported to the nucleus whereas NPM–ALK homodimers remain within the cytoplasm (30). In contrast, other fusions do not localize in the nucleus and do not show a nuclear staining pattern in anti-ALK immunohistochemistry. Interestingly, each ALK fusion usually has its own characteristic anti-ALK immunohistochemical staining pattern, because the subcellular localization of ALK fusions is dependent on the corresponding fusion partners. Anti-ALK immunohistochemistry has thus become a highly useful tool for both research and diagnostic purposes.

Since the discovery of EML4–ALK fusion in lung cancer (20), however, an unexpected problem in anti-ALK immunohistochemistry has become apparent, that is, the inability to detect a low level of fusion expression. To overcome this, we developed the intercalated antibody-enhanced polymer (iAEP) method, which moderately raises sensitivity in the immunohistochemical detection system (21). With this very simple method, anti-ALK immunohistochemistry has become a potent weapon in the diagnosis of EML4–ALK-positive lung cancer (21, 31–33). Other researchers used an anti-ALK rabbit monoclonal antibody, which is usually more sensitive than mouse monoclonal antibody, which can stain EML4–ALK (34). However, most EML4–ALK-positive lung cancer tissues do not stain well with conventional anti-ALK immunohistochemical methods because of the low message/protein level of EML4–ALK (21, 35). The expression level of a fusion gene depends on the promoter activity of the 5′-side gene, and that of EML4 is likely to be lower than that of the other ALK fusion partner genes, which may explain why EML4–ALK had not been discovered until 12 years after the development of the first anti-ALK antibody became available for immunohistochemistry (36). In other words, a tumor that immunostains for ALK only by a sensitive immunohistochemistry method may harbor a novel ALK fusion. Interestingly, in this study, we detected 2 IMT cases positive for ALK immunohistochemistry only when stained by iAEP method (21), and successfully identified a novel fusion gene, protein-tyrosine phosphatase, receptor-type, F polypeptide-interacting protein-binding protein 1 (PPFIBP1)–ALK.

Materials and Methods

Materials

Pathologic specimens from 2 pulmonary IMT cases, originally diagnosed as fibrous histiocytoma (1988: case 1, 45-year-old male; 1998: case 2, 34-year-old female), were reassessed morphologically and immunohistochemically. Surgically removed tumor specimens were routinely fixed in 20% neutralized formalin and embedded in paraffin for conventional histopathologic examination. For case 2, total RNA was extracted from the corresponding snap-frozen specimen and purified with the use of an RNeasy Mini kit (Qiagen). The study was approved by the institutional review board of the Japanese Foundation for Cancer Research.

Immunohistochemistry

Formalin-fixed, paraffin-embedded tissue was sliced at a thickness of 4 μm, and the sections were placed on silane-coated slides. For antigen retrieval, the slides were heated for 40 min at 97°C in Target Retrieval Solution (pH 9.0; Dako). For the conventional staining procedure, the slides were incubated at room temperature with Protein Block Serum-free Ready-to-Use solution (Dako) for 10 minutes and then with primary antibodies against ALK (5A4), smooth muscle actin, muscle-specific actin (HHF35), CD34, cytokeratins (AE1/AE3), S100, or desmin for 30 minutes. The immune complexes were then detected with dextran polymer reagent (EnVision + DAB system; Dako) and an AutoStainer instrument (Dako). The iAEP method was also used for the sensitive detection of ALK, as described previously (21).